

Review

Bridging Materials and Analytics: A Comprehensive Review of Characterization Approaches in Metal-Based Solid-State Hydrogen Storage

Yaohui Xu ^{1,3}, Yang Zhou ^{2,*} , Yuting Li ⁴ and Yang Zheng ^{5,*}

¹ Laboratory for Functional Materials, School of New Energy Materials and Chemistry, Leshan Normal University, Leshan 614000, China

² State Key Laboratory of New Textile Materials and Advanced Processing Technology, School of Textile Science and Engineering, Wuhan Textile University, Wuhan 430200, China

³ Leshan West Silicon Materials Photovoltaic New Energy Industry Technology Research Institute, Leshan 614000, China

⁴ College of Materials Science and Engineering, National Engineering Research Center for Magnesium Alloys, Chongqing University, Chongqing 400044, China

⁵ The State Key Laboratory of Refractories and Metallurgy, Institute of Advanced Materials and Nanotechnology, Wuhan University of Science and Technology, Wuhan 430081, China

* Correspondence: yzhou@wtu.edu.cn (Y.Z.); yzheng@wust.edu.cn (Y.Z.)

Abstract: The advancement of solid-state hydrogen storage materials is critical for the realization of a sustainable hydrogen economy. This comprehensive review elucidates the state-of-the-art characterization techniques employed in solid-state hydrogen storage research, emphasizing their principles, advantages, limitations, and synergistic applications. We critically analyze conventional methods such as the Sieverts technique, gravimetric analysis, and secondary ion mass spectrometry (SIMS), alongside composite and structure approaches including Raman spectroscopy, X-ray diffraction (XRD), X-ray photoelectron spectroscopy (XPS), scanning electron microscopy (SEM), transmission electron microscopy (TEM), and atomic force microscopy (AFM). This review highlights the crucial role of in situ and operando characterization in unraveling the complex mechanisms of hydrogen sorption and desorption. We address the challenges associated with characterizing metal-based solid-state hydrogen storage materials discussing innovative strategies to overcome these obstacles. Furthermore, we explore the integration of advanced computational modeling and data-driven approaches with experimental techniques to enhance our understanding of hydrogen–material interactions at the atomic and molecular levels. This paper also provides a critical assessment of the practical considerations in characterization, including equipment accessibility, sample preparation protocols, and cost-effectiveness. By synthesizing recent advancements and identifying key research directions, this review aims to guide future efforts in the development and optimization of high-performance solid-state hydrogen storage materials, ultimately contributing to the broader goal of sustainable energy systems.

Keywords: solid-state hydrogen storage materials; characterization techniques; hydrogen storage performance; structure and composition



Citation: Xu, Y.; Zhou, Y.; Li, Y.; Zheng, Y. Bridging Materials and Analytics: A Comprehensive Review of Characterization Approaches in Metal-Based Solid-State Hydrogen Storage. *Molecules* **2024**, *29*, 5014. <https://doi.org/10.3390/molecules29215014>

Academic Editor: Maurizio Peruzzini

Received: 19 September 2024

Revised: 14 October 2024

Accepted: 17 October 2024

Published: 23 October 2024



Copyright: © 2024 by the authors. Licensee MDPI, Basel, Switzerland. This article is an open access article distributed under the terms and conditions of the Creative Commons Attribution (CC BY) license (<https://creativecommons.org/licenses/by/4.0/>).

1. Introduction

The quest for clean and sustainable energy solutions has propelled the development of solid-state hydrogen storage materials to the forefront of scientific research [1–3]. These materials offer several advantages over traditional compressed or liquefied hydrogen storage methods, including higher storage capacities, improved safety, and ease of handling [4–6]. However, the complex nature of hydrogen storage mechanisms and the diverse range of materials being investigated present significant challenges in understanding their behavior and optimizing their performance [7–9].

To advance solid-state hydrogen storage materials from laboratory research to practical application, a comprehensive understanding of the microstructure, compositional changes, and dynamic behavior during hydrogenation/dehydrogenation processes is essential, and this is precisely where characterization techniques play a critical role [10,11]. For instance, techniques like the Sieverts method and gravimetric analysis are excellent for measuring the hydrogen storage capacity and kinetic behavior of materials, but when it comes to analyzing microstructural changes, they need to be complemented by optical and surface analysis techniques such as X-ray diffraction (XRD), Raman spectroscopy, and X-ray photoelectron spectroscopy (XPS). Additionally, neutron scattering is advantageous for studying the distribution and dynamic behavior of hydrogen atoms, while electrochemical methods are particularly effective in analyzing the electronic structure and surface reactivity of materials [12–18].

In recent years, with the continuous advancement of materials science, metal-based hydrogen storage materials have become a research hotspot due to their unique structures and excellent hydrogen storage performance [19–22]. These novel materials demonstrate outstanding potential for hydrogen storage, particularly in terms of increasing storage density and adsorption/desorption rates. However, the structural and performance complexity of these materials presents new challenges for characterization [23–26]. Traditional characterization techniques have certain limitations in terms of precision, sensitivity, and applicability, making it difficult to fully reveal the dynamic behavior of these new materials during the hydrogen storage process [27]. It is important to note that there is typically no “optimal” technique when selecting and applying characterization methods. Each technique has its strengths in revealing specific properties of materials, but they are also accompanied by limitations [28–30]. Thus, different characterization methods often complement and synergize with one another.

In summary, characterization techniques for solid-state hydrogen storage materials are key tools for understanding and optimizing their performance. We have conducted a comprehensive review of various characterization methods, aiming to provide researchers with a thorough technical reference that encompasses both traditional and emerging methods. By comparing the advantages and limitations of different techniques in their applications, we emphasize their complementarity and synergistic relationships, rather than seeking the so-called “optimal” testing method. Each characterization technique has its unique applicable scenarios and focal points, and no single method can fully elucidate all the mechanisms involved in hydrogen storage within solid-state materials. Therefore, this review particularly focuses on the unique demands of characterizing these novel materials and discusses how existing techniques can be improved or new methods developed to address these challenges. This review not only provides researchers with a comprehensive technical overview of the field of solid-state hydrogen storage characterization but also highlights the difficulties in characterizing emerging materials and the trends for future technological development. Through an in-depth analysis of various characterization techniques, we hope to provide a theoretical basis and technical support for achieving efficient and sustainable hydrogen storage solutions, thereby contributing to the continued development and application of clean energy technologies.

2. Hydrogen Storage Performance Characterization Techniques

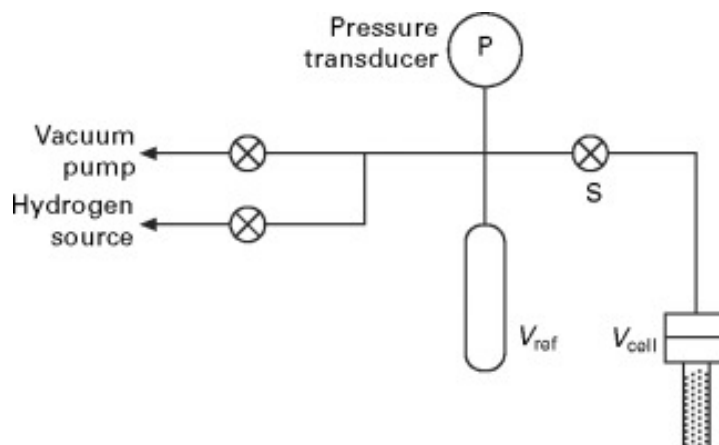
Hydrogen storage materials are crucial for advancing hydrogen-based energy systems, and their performance is highly dependent on their physical and chemical properties [31]. To thoroughly understand these materials, several fundamental characterization techniques are employed. The Sieverts method, gravimetric analysis, secondary ion mass spectrometry, neutron scattering, and electrochemical methods represent some of the most essential tools in this domain. By leveraging these methods, researchers can systematically evaluate and optimize hydrogen storage materials to meet the demands of practical applications in energy storage and conversion. Table 1 briefly summarizes the pros and cons of each basic characterization technique.

Table 1. The advantages and limitations of essential characterization techniques.

Method	Advantages	Limitations	Refs.
Sieverts method	Simplicity and reliability, measures hydrogen sorption isotherms, provides thermodynamic information	Sensitivity to volume calibration and leaks, limited information on kinetics, requires accurate temperature control	[26,30,32–40]
Gravimetric analysis	High sensitivity, real-time monitoring of hydrogen sorption, enables kinetic studies	Sensitivity to buoyancy effects, influence of impurities and adsorbed species, requires careful calibration and correction procedures	[39,40]
Thermogravimetric analysis Differential scanning calorimetry	Simultaneously measure changes in mass and heat flow, providing comprehensive information about thermal stability, decomposition, and phase transitions of materials in a single experiment	Limited sensitivity in detecting small mass changes and subtle thermal events, making them less suitable for analyzing materials with very low levels of thermal degradation or phase change	[41–48]
Secondary ion mass spectrometry	High spatial resolution, sensitive to low hydrogen concentrations, provides depth profiling information	Destructive technique, requires careful calibration for quantitative analysis, challenging data interpretation due to matrix effects	[49–58]
Electrochemical methods	Simulates real-world operating conditions, provides information on charge–discharge behavior and kinetics, enables the study of cycle stability and long-term performance	Sensitivity to electrode preparation and cell configuration, requires careful interpretation of electrochemical data, may not provide direct structural and chemical information	[59–71]

2.1. Sieverts Method

The Sieverts method, also known as the volumetric method, is one of the most widely used techniques for characterizing hydrogen storage materials [32,33]. The core principle is based on the ideal gas law and the pressure changes during the gas absorption and desorption processes. The simplified schematic of the device is shown in Figure 1 [34]. When high-pressure gas comes into contact with a metal sample, the gas dissolves into the metal. According to Henry’s law, the solubility of the gas in the metal is proportional to the partial pressure of the gas. By measuring the pressure changes before and after gas injection with a high-precision pressure sensor system, the amount of gas dissolved in the metal sample can be calculated.

**Figure 1.** Schematic representation of a Sieverts apparatus [34].

The Sieverts method offers several advantages, including simplicity, reliability, and the ability to measure hydrogen sorption isotherms over a wide range of pressures and temperatures [35]. It provides essential thermodynamic information, such as the equilibrium pressure, enthalpy, and entropy of the hydrogen sorption reactions [36]. To overcome the limitations of the Sieverts method, researchers have developed advanced apparatus with improved temperature control, high-precision pressure sensors, and automated data acquisition systems. The Sieverts method is widely utilized in mainstream hydrogen testing and analysis instruments for analyzing hydrogen storage density in hydrogen storage materials. This technique provides essential measurements of hydrogen absorption and desorption capacities, critical for evaluating material performance in hydrogen storage applications [26,30]. Rigorous calibration procedures and error analysis methods have been implemented to enhance the accuracy and reliability of the measurements. The Sieverts method is particularly crucial for evaluating the hydrogen storage capacity and kinetics of metal hydrides.

Existing volumetric measurement instruments often suffer from low efficiency due to insufficient calibration techniques, temperature gradients, and limited automation. As shown in Figure 2a, the curve changes with the temperature of the sample. As the sample temperature increases, the line moves further from the sample cell, resulting in an increase in the apparent volume of the sample cell and a decrease in the apparent volume of the tube. The position of this line can be determined through calibration methods and is defined as a function of temperature. Zhu et al. [38] proposed a novel volumetric calibration and thermal gradient resistance method by introducing a continuous function to overcome temperature gradients across the entire test temperature range. This method was validated through TPD/TPA tests on MgH_2 powder, demonstrating automatic temperature control. Moreover, the new method enabled the completion of three PCT curves within 1.5 days. This innovative approach has the potential to make Sieverts instruments more effective, accurate, and reliable tools for characterizing hydrogen storage materials.

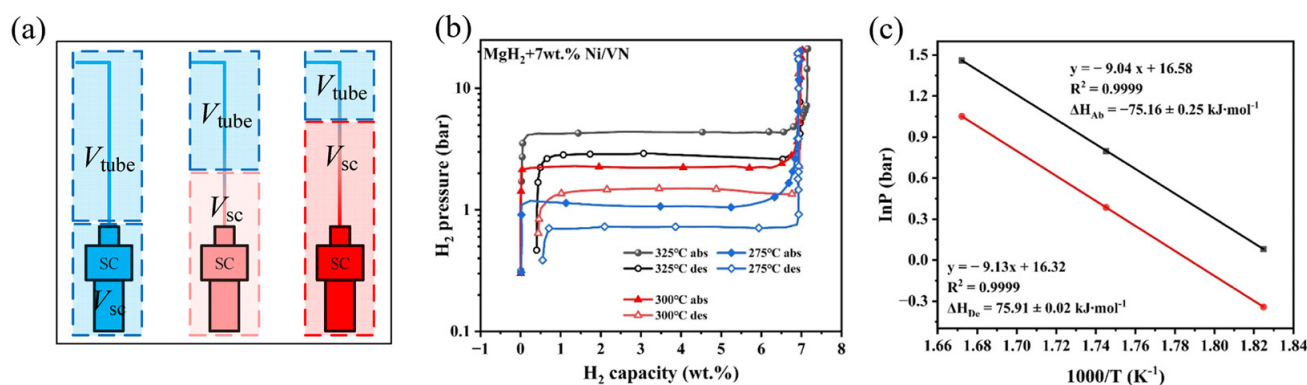


Figure 2. (a) Diagram of temperature gradients in the reactor [38]. The $\text{MgH}_2 + 7 \text{ wt.}\% \text{ Ni/VN}$ (b) PCT curves at 325 and 275 °C and (c) Van't Hoff plots [72].

The PCT curve is primarily used to describe the relationship between the composition of a chemical system and pressure under isothermal conditions, and it is commonly applied in the study of gas adsorption and metal hydrides for hydrogen storage. By analyzing the PCT curve, insights can be gained into the phase behavior of the system, adsorption or desorption processes, and the hydrogen storage capacity of the material. The van't Hoff equation $\ln K = -\Delta H/RT + \Delta S/R$, where K is the equilibrium constant, ΔH is the standard reaction enthalpy ($\text{kJ}\cdot\text{mol}^{-1}$), ΔS is the standard reaction entropy ($\text{J}\cdot\text{mol}^{-1}\cdot\text{K}^{-1}$), R is the gas constant ($\text{J}\cdot\text{mol}^{-1}\cdot\text{K}^{-1}$), and T is the temperature (K), reveals the relationship between the chemical equilibrium constant and temperature, forming the theoretical foundation for studying the effect of temperature on equilibrium in reaction thermodynamics. Wu et al. [72] measured the PCT curves of $\text{MgH}_2 + 7 \text{ wt.}\% \text{ Ni/VN}$ and ball-milled MgH_2 samples at different temperatures (Figure 2b). The results show that the plateau pressures for

MgH₂-7 wt.% Ni/VN during desorption at 548, 573, and 598 K were 0.72, 1.49, and 2.90 bar, respectively, and during absorption, the plateau pressures were 1.10, 2.25, and 4.20 bar, respectively. For ball-milled MgH₂, the desorption plateau pressures at 598, 623, and 648 K were 2.20, 4.12, and 7.40 bar, respectively, while the absorption pressures were 3.82, 7.00, and 12.20 bar. Using the van't Hoff equation to calculate the ΔH for hydrogen absorption and desorption of MgH₂-7 wt.% Ni/VN at different temperatures based on the plateau pressures, the values were found to be -75.16 ± 0.25 and 75.91 ± 0.02 kJ·mol⁻¹ (Figure 2c), indicating no significant reduction compared to pure MgH₂.

By experimentally determining the changes in the equilibrium constant with temperature, thermodynamic parameters such as enthalpy and entropy changes can be obtained. The van't Hoff equation not only helps in understanding the influence of temperature on the direction and extent of chemical reactions but also has wide applications in material design, catalysis, and industrial process optimization. The combination of the PCT curve and the van't Hoff equation allows for in-depth study of thermodynamic behavior in multi-phase systems such as gas–solid and liquid–solid phases, providing reliable thermodynamic parameters to optimize material performance and understand reaction mechanisms.

2.2. Gravimetric Analysis

Gravimetric analysis is another fundamental technique for characterizing hydrogen storage materials. It involves measuring the mass change of a sample during hydrogen absorption or desorption processes [39]. One of the main advantages of gravimetric analysis is its high sensitivity, allowing for the detection of small mass changes associated with hydrogen sorption. It provides real-time monitoring of the hydrogen uptake and release, enabling the study of kinetics and the determination of the rate-limiting steps in the sorption processes [40]. Gravimetric analysis offers unique advantages in studying hydrogen storage materials, particularly for understanding sorption kinetics and cycling stability. However, due to the high cost of high-temperature magnetic levitation balances, this method is rarely used in the practical analysis of hydrogen storage materials.

Thermogravimetric analysis (TG) is a method used to measure changes in the mass of a sample as the temperature increases or under isothermal conditions [42,44]. TG is usually combined with differential scanning calorimetry (DSC), which detects the heat flow difference between the sample and a reference during heating or cooling, revealing the endothermic or exothermic behavior of the material and the thermal decomposition process [45,47]. The advantage of TG-DSC technology lies in its ability to simultaneously acquire both mass changes and heat flow information, offering a more comprehensive view of the material's physical and chemical behavior at various temperatures [41,43,46]. TG-DSC precisely characterizes the decomposition temperature and exothermic or endothermic properties of composite materials, helping to determine thermal stability and processing parameters. For hydrogen storage materials, by applying the Kissinger equation ($\ln(\beta/T_p^2) = \ln(AR/E_a) - E_a/(RT_p)$), where β is the heating rate (K/min), T_p is the desorption peak temperature (K), R is the gas constant (J/mol·K), E_a is active energy (kJ/mol), and A is the frequency factor, to fit the TG-DSC results, the activation energy of hydrogen desorption can be analyzed, providing insights into the kinetic properties of the material. Xiao et al. [48] measured the DSC curve of samples and found that after doping MgH₂ with Ce_{0.6}Zr_{0.4}O₂, the desorption peak temperature decreased compared to that of ball-milled MgH₂ alone (Figure 3a). Two adjacent endothermic peaks appeared on the DSC curve: the first lower-temperature desorption peak was attributed to the activation of MgH₂ catalyzed by Ce_{0.6}Zr_{0.4}O₂, while the second higher-temperature peak was due to non-activated MgH₂. The Kissinger equation (Figure 3b) was used to calculate the activation energy for the first low-temperature desorption peak of MgH₂-7CeZrO, which was approximately 66.85 kJ/mol, about 45% lower than that of ball-milled MgH₂ 121.07 kJ/mol. In addition, the activation energy $De-E_a$ of MgH₂-7CeZrO was 116.06 kJ/mol by fitting the second dehydrogenation peak of MgH₂-7CeZrO, indicating that $De-E_a$ was close to $De-E_a$ after MgH₂ grinding, confirming the explanation that the second peak was inactive MgH₂.

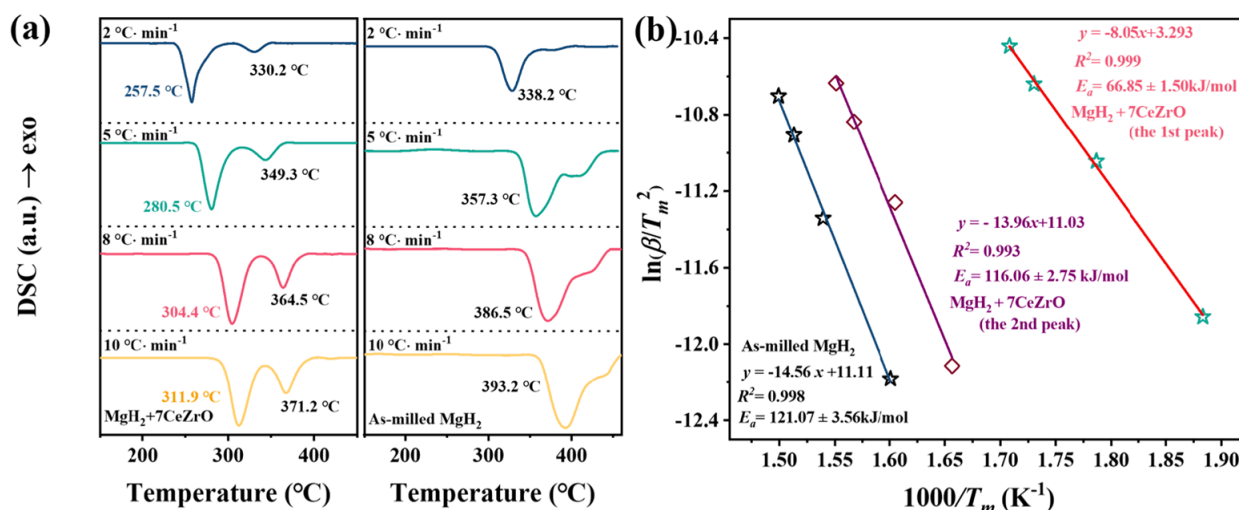


Figure 3. (a) The DSC profiles at 2, 5, 8, and 10 $^\circ\text{C}\cdot\text{min}^{-1}$ of $\text{MgH}_2\text{-7CeZrO}$ and ball-milled MgH_2 ; (b) the apparent dehydrogenation activation energy of $\text{MgH}_2\text{-7CeZrO}$ and undoped MgH_2 by Kissinger equation.

Although TG-DSC is highly effective in analyzing the hydrogen desorption kinetics of hydrogen storage materials, it should be noted that this method cannot monitor the hydrogen absorption process.

2.3. Secondary Ion Mass Spectrometry

Secondary ion mass spectrometry (SIMS) is a powerful surface characterization technique that provides detailed information about the elemental composition and distribution of hydrogen in storage materials [49,50]. As illustrated in Figure 4, SIMS involves bombarding the sample surface with a high-energy ion beam, producing secondary ions. These secondary ions are separated and detected by a mass spectrometer based on their mass-to-charge ratio (m/z), providing information about the composition and structure of the sample surface (Figure 4a). The primary ions (such as Cs^+ or O^{2+}) bombard the sample surface, causing sputtering of the surface material and generating secondary ions [51]. The production rate of secondary ions depends on the surface concentration of the sample and the sputtering yield of the primary ions (Figure 4b). By separating and detecting the secondary ions with a mass spectrometer, the composition and structure of the sample surface elements can be determined (Figure 4c).

The different binding energies of hydrogen atoms make the analysis of hydrogen storage processes in carbon-containing materials extremely complex. To differentiate between surface atoms and atoms embedded in the sample, Madroñero et al. [52] used a SIMS spectrometer with periodic ion beam interruption, observing some outgassing phenomena of surface hydrogen under room temperature and high-vacuum conditions. SIMS has proven invaluable in studying the spatial distribution of hydrogen and other elements in complex storage materials. For example, D. Andersen et al. [53] combined SIMS with dual-beam focused ion beam scanning electron microscopy to obtain high-resolution imaging of hydrogen and deuterium in $\text{Mg}_2\text{Ni}/\text{Mg}_2\text{NiH}_4$ hydrogen storage films. This allowed successful characterization of the formation process of hydrides at different depths in the films, providing valuable insights into the hydrogen storage mechanisms of the materials. When the grains exhibit an equiaxed structure (Figures 4c and 5a), hydrides mainly form on the film surface, evidenced by an enhanced ^1H signal in the surface “hydride” local depth profile. In contrast, when the grains exhibit a columnar structure (Figure 5b,d), the hydrides extend toward the substrate, forming a continuous region. The local depth profile shows that the fully hydride layer is confined near the substrate and is surrounded by a sub-hydride layer.

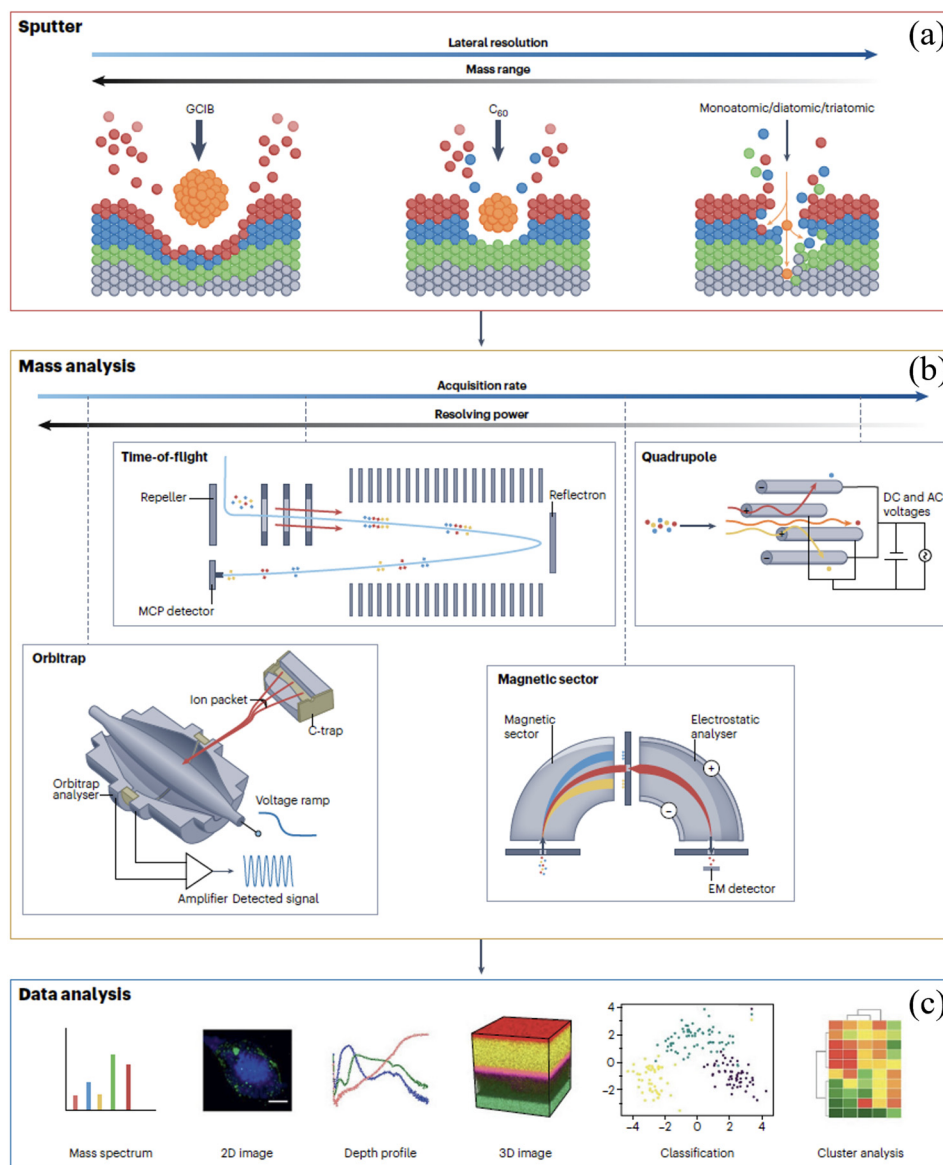


Figure 4. A schematic overview of the secondary ion mass spectrometry experiment [51]. (a) A surface is bombarded with a primary ion resulting in the sputtering of secondary ions characteristic of surface chemistry. Secondary ions are detected and measured by mass spectrometry. The bombardment is by primary ions, ranging from atomic ions offering the highest lateral resolution to massive gas cluster ion beams that liberate surface species up to several thousand mass units. (b) Mass analysis of secondary ions is generally by quadrupole magnetic sector, time-of-flight, or Orbitrap instruments. (c) Outputs from the analysis include mass spectra, 2D or 3D images, and depth profiles, which can be further processed using machine learning. EM, electromagnetic; MCP, microchannel plate [51].

Although SIMS technology is not extensively employed currently in the analysis of solid-state hydrogen storage materials, its unique advantages, including high spatial resolution, sensitivity to hydrogen concentrations as low as parts per million (ppm), and capability to provide depth profile information, offer significant potential. In the future, SIMS could play a crucial role in supplementing the characterization of hydrogen storage materials, addressing existing gaps in understanding various aspects of these materials [54,55]. To overcome the limitations of SIMS, advanced instrumentation with improved mass resolution and sensitivity has been developed [56]. The use of multi-modal SIMS, combining different primary ion beams and detection modes, has enhanced the capabilities of the

technique [57]. Careful sample preparation and the use of appropriate reference materials are essential for accurate quantification [58].

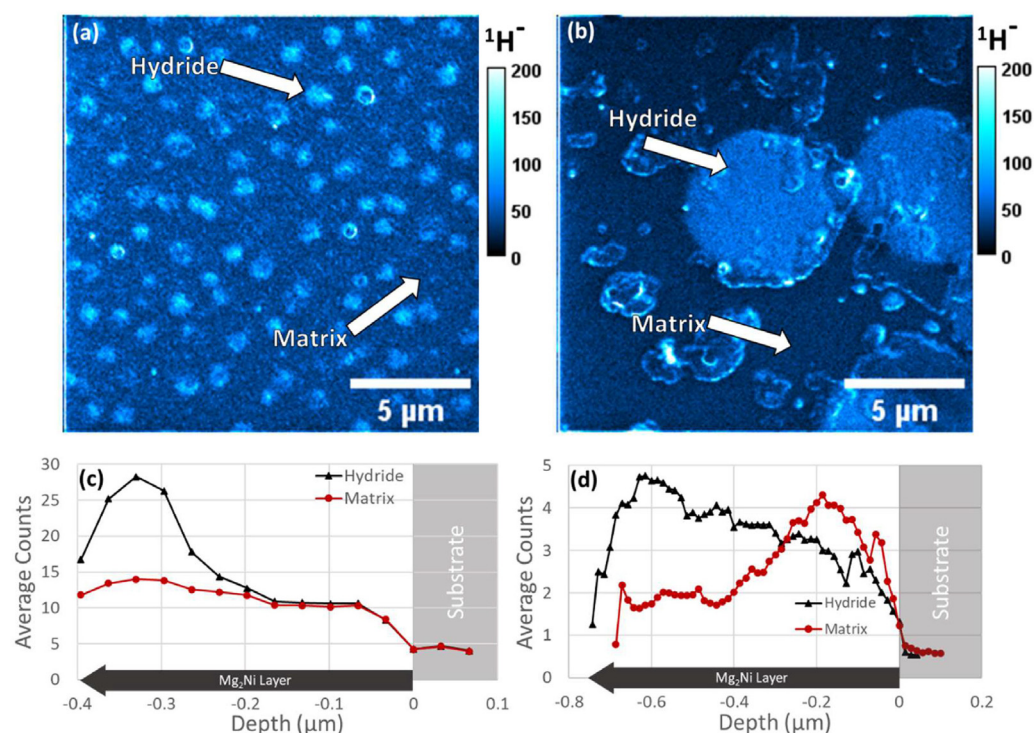


Figure 5. SIMS images from a hydrogenated sample with (a) equiaxed microstructure (*Batch A—Sample 1*) showing the summed signal over 3 slices and (b) columnar microstructure (*Batch B—Sample 2*) showing the summed signal over 14 slices. SIMS localized depth profiles from regions inside and outside of the surface-visible hydride areas for (c) *Sample 1* and (d) *Sample 2*. Note that for (d), the “hydride” data have been shifted to correct its depth so that both curves agree on the depth of the substrate (zero on the x-axis), since the hydrides stick above the surface (discussed below). For (a,c), 15 total slices were captured with an average slice thickness of 33 nm. Beam current of 50 pA and a dwell time of 4 ms per pixel. Image resolution of 256×256 pixels for FOV of $17 \times 17 \mu\text{m}$. For (b,d), 56 slices total were collected with an average slice thickness of 14.3 nm. Beam current of 100 pA and a dwell time of 1 ms per pixel. Image resolution of 256×256 pixels for FOV of $17 \times 17 \mu\text{m}$ [53].

2.4. Electrochemical Characterization Methods

Electrochemical methods, including cyclic voltammetry, chronopotentiometry, and electrochemical impedance spectroscopy, are valuable tools for characterizing the electrochemical hydrogen storage properties of materials [59,60]. These techniques provide insights into the charge–discharge behavior, kinetics, and reversibility of hydrogen sorption processes in electrochemical systems, such as metal hydride batteries [61–63].

Cyclic voltammetry involves sweeping the potential of the working electrode containing the hydrogen storage material and measuring the resulting current. Chronopotentiometry applies a constant current to the electrode and monitors the potential response over time [64]. Electrochemical impedance spectroscopy (EIS) measures the impedance of the electrochemical system over a wide range of frequencies [65]. To overcome the limitations of electrochemical methods, researchers have developed advanced electrochemical cell designs and measurement protocols. The use of reference electrodes and optimized electrolyte compositions can improve the accuracy and reliability of the measurements [66]. Combining electrochemical methods with other characterization techniques, such as XRD and Raman spectroscopy, can provide a more comprehensive understanding of the electrochemical hydrogen storage behavior. The operational principle of nickel–metal hydride (NiMH) batteries fundamentally involves the absorption and desorption of hydrogen

by metal hydrides. This principle can be similarly exploited through electrochemical methods to swiftly assess the performance characteristics of solid-state hydrogen storage materials [67–70]. Edalati et al. [71] discovered that $\text{Ti}_x\text{Zr}_{2-x}\text{CrMnFeNi}$ alloys, benefiting from the Ti/Zr ratio of the C14 Laves structure, exhibit good room-temperature hydrogenation/dehydrogenation capabilities. Electrochemical tests on their discharge potential, discharge capacity, and discharge capacity versus cycle number showed that this high-entropy alloy (HEA) successfully functions as the negative electrode of a nickel–metal hydride battery, with excellent charge–discharge cycling performance. The optimal Ti/Zr ratio achieved the highest storage capacity and fastest activation.

3. Structure and Composition Characterization Techniques

As the field of hydrogen storage materials evolves, advanced spectroscopic and microscopic techniques have become indispensable for detailed characterization at the molecular and atomic levels [73]. Techniques such as Raman spectroscopy, X-ray diffraction, and X-ray photoelectron spectroscopy offer unparalleled capabilities in probing the structural, electronic, and chemical properties of hydrogen storage materials. These advanced techniques enable researchers to achieve a deeper understanding of the interactions and mechanisms at play within these materials, facilitating the development of more efficient and robust hydrogen storage solutions. By employing these sophisticated methods, scientists can gain comprehensive insights that drive innovation and optimization in the design and application of hydrogen storage materials. Table 2 briefly summarizes the pros and cons of various spectroscopic and microscopic techniques.

Table 2. The advantages and limitations of advanced spectroscopic and microscopic techniques.

Method	Advantages	Limitations	Refs.
Raman spectroscopy	Non-destructive and non-contact technique, high spectral resolution, identifies different hydrogen-bonding configurations	Sensitivity to sample surface and orientation, challenging interpretation for complex materials, may not provide quantitative hydrogen content information	[74–85]
Fourier transform infrared spectroscopy	Rapid, non-destructive detection with high sensitivity to low-concentration molecular vibrations; wide range of organic and inorganic materials; excels in identifying functional groups and chemical bonds	It is sensitive to moisture, with water absorption peaks potentially interfering with analysis. It only detects infrared-active functional groups, making non-polar bond vibrations difficult to observe.	[37,86–91]
X-ray diffraction	Crystalline Structure Determination, wide range of materials, Phase Identification	Limited to Crystalline Materials, Penetration Depth, Size Limitation	[92–105]
Neutron scattering techniques	Non-destructive technique, provides bulk structural and dynamic information, sensitive to light elements like hydrogen	Requires access to specialized neutron sources, complex data interpretation, challenging sample preparation	[106–112]
X-ray photoelectron spectroscopy	Surface-sensitive technique, provides elemental composition and chemical state information, investigates surface catalysts and coatings	Limited information on bulk properties, requires clean and well-defined sample surface, may not provide direct hydrogen content information	[113–123]
Scanning electron microscopy	High-resolution surface imaging, large depth of focus, suitable for three-dimensional topography observation, simple sample preparation	Can only observe surface structures; cannot provide internal structural information; may require metal coating, which affects the true morphology	[124–132]

Table 2. Cont.

Method	Advantages	Limitations	Refs.
Atomic force microscopy	Ultra-high resolution, reaching atomic level; does not require a vacuum environment, allowing for observation of live samples; capable of measuring mechanical and electrical properties of materials	Slow scanning speed, suitable for small area samples; influenced by probe shape, which may cause artifacts; requires surface flattening treatment of the sample	[133–138]
Transmission and scanning transmission electron microscopy	Extremely high resolution, capable of observing atomic-level structures; can provide internal structural information of samples; able to perform compositional and phase analysis	Samples must be very thin; complex sample preparation, which may introduce artifacts; requires a vacuum environment, potentially causing sample damage	[139–148]

3.1. Composition Characterization Techniques

3.1.1. Raman and Fourier Transform Infrared Spectroscopy

Raman spectroscopy has emerged as a powerful technique for investigating the local structure, bonding, and vibrational properties of hydrogen in storage materials [74,75]. When monochromatic light (usually a laser) illuminates a sample, photons interact with molecules, producing scattered light. A portion of this scattered light undergoes a frequency shift (Raman scattering), which provides information on molecular vibrations and rotations. When the laser illuminates the sample, most photons undergo Rayleigh scattering (elastic scattering with no frequency shift), but a small number of photons undergo Raman scattering (inelastic scattering), with their frequencies shifted due to changes in molecular vibrational or rotational energy levels. Raman-active molecules located near waveguides can be excited through either in-plane coupling (waveguide mode) or out-of-plane coupling (as depicted in Figure 6a). In “classical” Raman scattering, emission typically occurs in the reverse direction to eliminate background interference from the excitation light (as illustrated in Figure 6b). This technique is particularly vital for studying amorphous hydrogen storage materials, providing crucial insights into their structural properties [76].

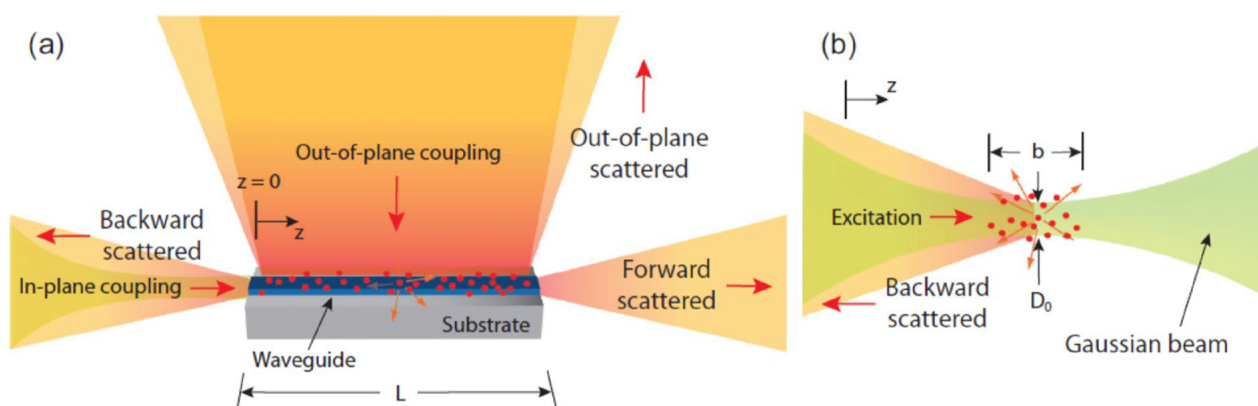


Figure 6. (a) Schematic of different configurations of laser excitation and Raman scattered light collection. (b) Schematic of laser excitation and Raman scattered light collection in free space [76].

Raman spectroscopy offers several advantages for characterizing hydrogen storage materials, including its non-destructive and non-contact nature, high spectral resolution, and the ability to identify different hydrogen-bonding configurations [77]. It is particularly useful for studying the interactions between hydrogen and the host material, such as the formation of metal–hydrogen bonds [78]. This technique is particularly vital for studying amorphous hydrogen storage materials, providing crucial insights into their structural

properties [79–81]. Raman spectroscopy has proven invaluable in studying the local structure and bonding in complex hydrides. Ross et al. [74] used this technique to investigate the decomposition pathway of sodium aluminum hydride (NaAlH_4), a promising hydrogen storage material. Their study revealed distinct Raman shifts associated with different Al-H bond configurations, providing insights into the dehydrogenation mechanism. Pedraza et al. [82] studied the mechanism of hydrogen release from ammonia borane within mesoporous materials using Raman spectroscopy and mass spectrometry. Figure 6a,b show that, at the point of maximum hydrogen evolution, the deformation mode of $-\text{NH}_3$ at 1601 cm^{-1} disappears, while two new modes emerge at 1565 cm^{-1} and 1085 cm^{-1} , indicating the formation of polymeric aminoborane (PAB). When the temperature reaches around 101°C , the intensity of these modes decreases significantly, along with other vibrational modes such as B-H, H-B-H, B-N, and N-B-H. At 50°C , the B-N stretching modes of ^{10}B and ^{11}B at 799 cm^{-1} and 783 cm^{-1} show a slight redshift (see inset in Figure 7), and around 106°C , they merge and diminish sharply, almost disappearing at 109°C . However, the mode near 783 cm^{-1} persists at higher temperatures and is associated with the B-N vibrational mode in polyaminoborane ($-\text{[BH}_2\text{NH}_2]^{n-}$), indicating the formation of this phase. Additionally, above 100°C and with Raman shifts higher than 3150 cm^{-1} , strong noise appears in the signal. The entire Raman spectrum undergoes significant changes around 106°C , with all vibrational modes weakening, while hydrogen release becomes highly significant in the online mass spectrometry analysis (Figure 7c).

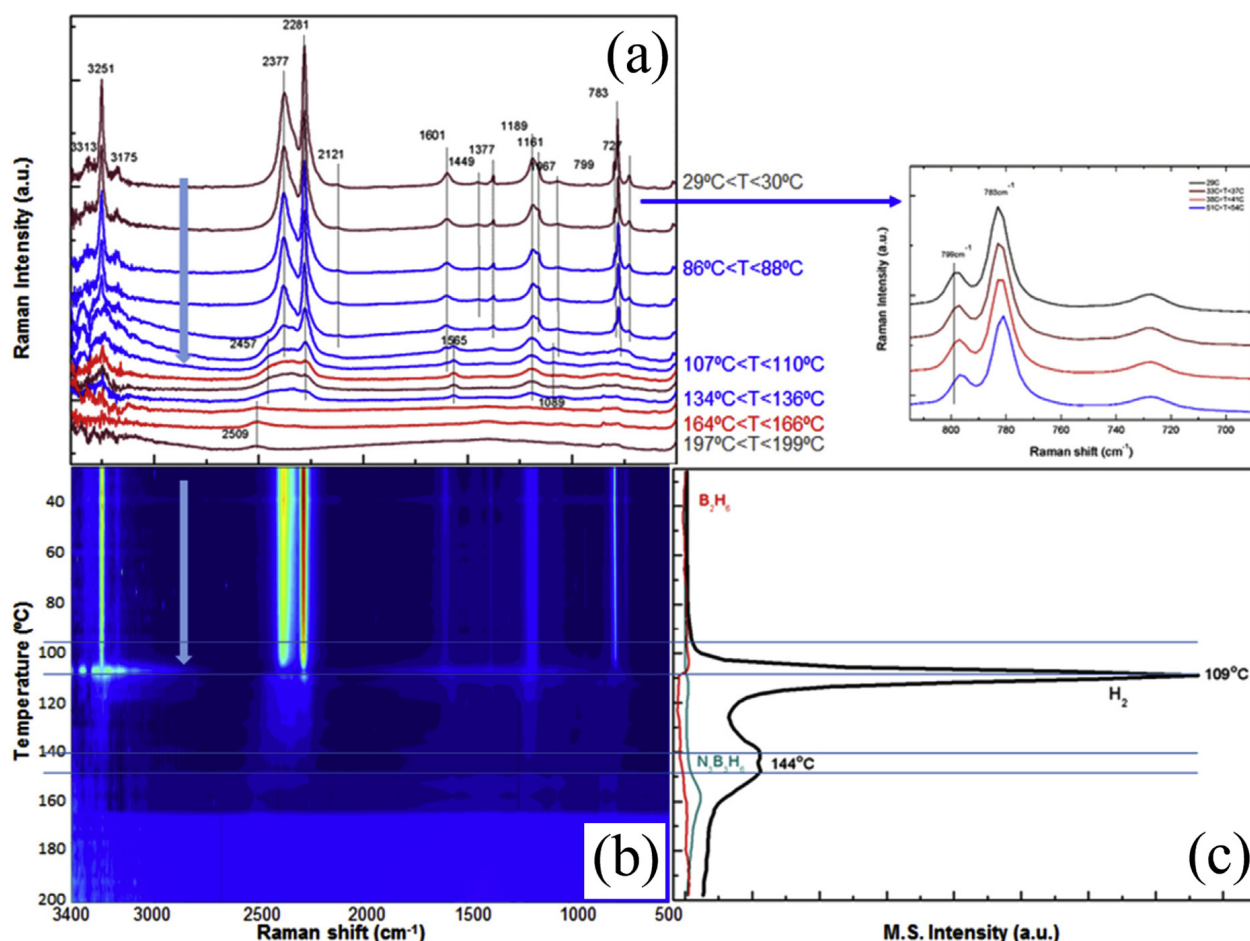


Figure 7. (a) Representative Raman spectra. (b) In situ Raman profile of materials under heating conditions (from room temperature to 200°C) and (c) simultaneous mass spectrometry profiles for H_2 and other volatile components evolved during thermal decomposition of neat AB under a ramp of $1^\circ\text{C}\cdot\text{min}^{-1}$ [82].

Fourier transform infrared spectroscopy (FTIR) is an analytical technique that studies the molecular composition and chemical structure of a sample by measuring the absorption or transmission of infrared spectra [89,91]. Different molecular functional groups exhibit specific absorption characteristics for particular wavelengths of infrared light [88,90]. FTIR identifies these characteristic absorption peaks, allowing for rapid, sensitive, and non-destructive qualitative and semi-quantitative analysis [86,87]. It is widely applied in fields such as chemistry, materials science, environmental monitoring, and pharmaceuticals.

In the study of coordination hydrides, FTIR plays a key role as it can accurately detect changes in molecular structure and chemical bonds. Coordination hydrides undergo dynamic changes in metal–hydrogen coordination bonds or hydride groups during hydrogen storage and release processes. FTIR can reveal the mechanisms of hydrogenation and dehydrogenation by monitoring the characteristic absorption peaks of these chemical bonds. By tracking the changes in M–H (metal–hydrogen) bond vibration frequencies, FTIR can directly follow the interactions between metal centers and hydrogen in coordination hydrides during hydrogen absorption and desorption. Different metal coordination centers (e.g., transition metals or rare-earth elements) and hydride combinations produce unique infrared absorption peaks, allowing FTIR to distinguish these changes and identify different hydrogen storage mechanisms. Ding et al. [37] utilized FTIR to investigate the hydrogen storage mechanism of the $\text{LiBH}_4\text{-MgH}_2$ system prepared via ball milling aerosol spraying (BMAS), as shown in Figure 8. Although the characteristic absorption of LiH at 1030 cm^{-1} overlaps with the absorption band of $\alpha\text{-Mg(BH}_4)_2$, the absorption bands of $\text{Mg(BH}_4)_2$ at 1262 and 1375 cm^{-1} almost disappeared in the 8R sample, while the absorption band at 1030 cm^{-1} remained visible, indicating the presence of LiH during the reaction process. This observation suggests that $\text{Mg(BH}_4)_2$ gradually decomposes over several dehydrogenation cycles, while LiH is formed through the reactions as follows: $12\text{LiBH}_4(\text{s}) = \text{Li}_2\text{B}_{12}\text{H}_{12}(\text{s}) + 10\text{LiH}(\text{s}) + 13\text{H}_2(\text{g})$ and $\text{Li}_2\text{B}_{12}\text{H}_{12}(\text{s}) + 6\text{MgH}_2(\text{s}) = 6\text{MgB}_2(\text{s}) + 2\text{LiH}(\text{s}) + 11\text{H}_2(\text{g})$. The gradual increase in the intensity of MgB_2 and LiH in the samples after cycling reflects the partial reversibility of the above reactions and further explains the gradual decline in hydrogen capacity of the BMAS powders during the cycling process.

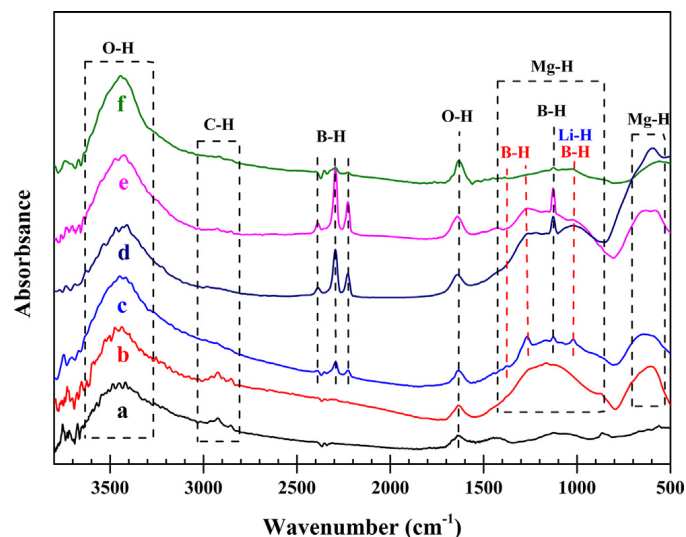


Figure 8. FTIR spectra of (a) the commercially purchased bulk KBr powder, (b) hand-mixed $\text{MgH}_2 + 5\text{ vol\% C}$, (c) BMAS powder, (d) BMAS powder after one dehydrogenation (1R) powder, (e) BMAS powder after one dehydrogenation and then re-hydrogenation (1S) powder, and (f) BMAS powder after 7 cycles of dehydrogenation and re-hydrogenation and then dehydrogenation again (8R) powder [37].

Raman spectroscopy is a key tool for studying the hydrogenation and dehydrogenation mechanisms of metal hydrides. By monitoring changes in Raman spectra during hydrogen

adsorption, insights into phase transitions, structural changes, and kinetics can be obtained. To fully exploit the potential of Raman spectroscopy, researchers have developed advanced instruments and data analysis methods, such as confocal Raman microscopy for high-resolution spatial mapping and in situ Raman spectroscopy for real-time monitoring of hydrogen adsorption processes. Alongside Raman spectroscopy, FTIR also plays an important role in hydrogen storage studies by detecting changes in chemical bonds between hydrogen and metal or metal oxide matrices, providing molecular vibrational information during hydrogen absorption and desorption.

These two techniques complement each other, with FTIR being particularly advantageous for detecting X-H (such as M-H or O-H) stretching vibrations in hydrides. In combination, Raman and FTIR spectroscopy provide a comprehensive analysis of material structures, chemical bond vibrations, and phase transitions, offering powerful tools for the design and optimization of hydrogen storage materials.

3.1.2. X-Ray Diffraction and Neutron Scattering

X-ray diffraction (XRD) is a fundamental technique for characterizing the crystallographic structure, phase composition, and structural changes in hydrogen storage material, and the schematic diagram is shown in Figure 9. Its fundamental equation is Bragg's law, which describes the conditions for XRD in a crystal. When X-rays illuminate a crystal, the atomic planes within the crystal cause the XRD [92,93]. By measuring the diffraction angles and intensities, one can determine the lattice parameters and atomic arrangement of the crystal [104,105]. Bragg's law reveals the relationship between the crystal structure and the X-ray wavelength, enabling the inference of the crystal's three-dimensional structure from its diffraction pattern [103].

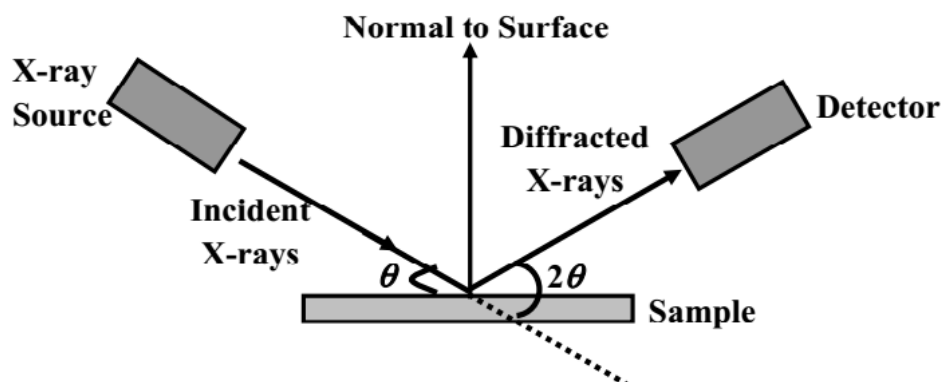


Figure 9. Schematic diagram of the XRD principle.

XRD is widely used in hydrogen storage research to investigate the structural properties of metal hydrides, complex hydrides, and other crystalline storage materials [94–96]. It allows for the identification of the hydrogen storage phases, the determination of the phase abundances, and the study of phase transitions during the hydrogen sorption processes. One of the advantages of XRD is its non-destructive nature, allowing for the characterization of the bulk properties of the material [97]. It provides statistical information about the average structure, complementing local probe techniques like Raman spectroscopy. In situ XRD has emerged as a powerful tool for studying the structural evolution of hydrogen storage materials during absorption and desorption cycles. Zlotea et al. [98] used in situ XRD to analyze the hydrogen release and absorption process of the TiZrNbHfTa high-entropy alloy. Through in situ XRD (Figure 10a,b), the phase transformations between the alloy, monohydride, and dihydride were observed clearly, greatly aiding researchers in understanding the dynamic hydrogen absorption and desorption processes of the alloy materials.

Furthermore, the advent of high-energy synchrotron X-ray sources has enabled rapid, time-resolved XRD measurements. Jensen et al. [99] leveraged this capability to study the dehydrogenation kinetics of NaAlH_4 , a promising complex hydride. Their millisecond-

resolution measurements uncovered transient phases that play a critical role in the hydrogen release process, demonstrating the power of advanced XRD techniques in elucidating complex reaction mechanisms.

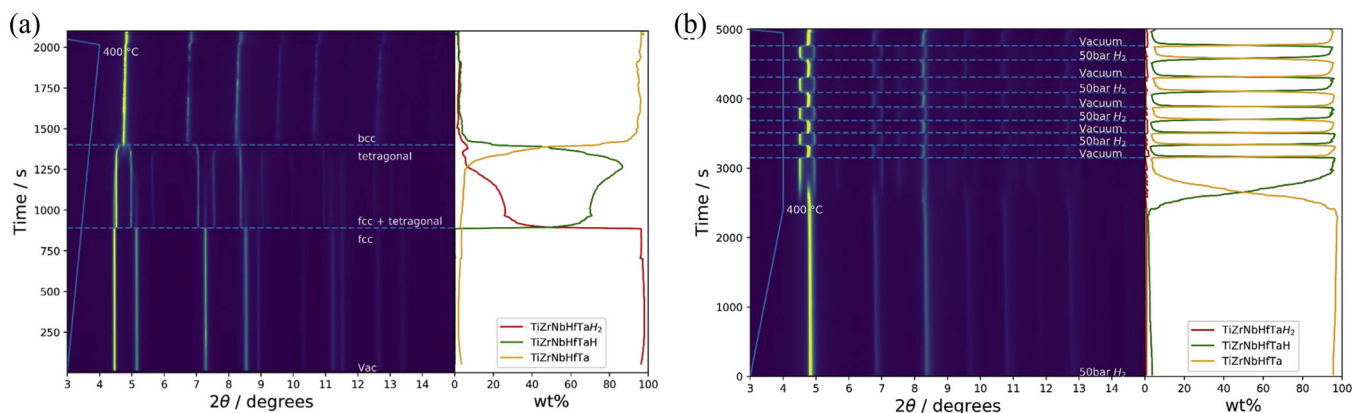


Figure 10. In situ SR-XRD and phase content at 400 °C during (a) hydrogen desorption in dynamic vacuum and (b) cycling between 50 bar H_2 and dynamic vacuum [98].

Neutron scattering techniques, including neutron diffraction and inelastic neutron scattering, are powerful tools for investigating the structural and dynamic properties of hydrogen in storage materials [100,101]. Neutron scattering involves the interaction of neutrons with the atomic nuclei in the material to study the structure and dynamics of the material. Neutron scattering includes elastic scattering (such as neutron diffraction) and inelastic scattering. When a neutron beam irradiates a sample, neutrons scatter off the sample's atomic nuclei, and the scattered neutrons are collected by detectors, as illustrated in Figure 11 [102]. By analyzing the angle and energy distribution of the scattered neutrons, information about the atomic structure and dynamics of the sample can be obtained.

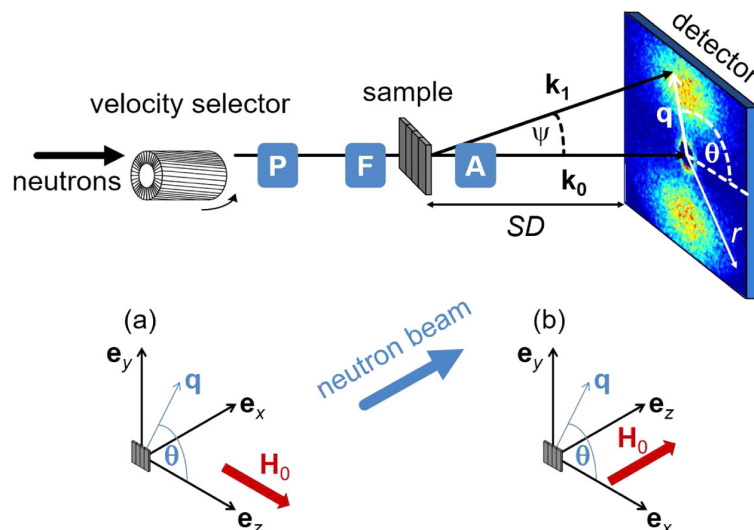


Figure 11. Schematic diagram of a neutron scattering device [102].

By measuring and analyzing the scattering cross-section and momentum transfer, the atomic structure and dynamics of the sample can be inferred. Neutrons have unique advantages for studying hydrogen, as they can penetrate deep into the material and have high sensitivity to light elements like hydrogen [106]. In situ neutron scattering can determine the reaction process of Mg-based hydrides by tracking phase changes and distributions during H_2 desorption and absorption reactions. Ponthieu et al. [107] studied

the reversible deuterium absorption of MgD_2 - TiD_2 nanocomposites using this technique. By examining the in situ H_2 desorption process, they found that the dehydrogenation peak of 0.3TiH_2 - 0.7MgH_2 appeared at 520 K, approximately 30 K lower than that of pure MgD_2 , and the desorption kinetics were significantly faster. They discovered that the transformation of $\beta\text{-MgD}_2$ to Mg is the only reversible loading path for deuterium at moderate pressure and temperature (i.e., $p < 1$ MPa, $T < 600$ K). The addition of TiD_2 not only restricted grain growth of the Mg and MgD_2 phases but also induced lattice distortion in $\beta\text{-MgD}_2$. The TiD_2 phase facilitated hydrogen migration through the sub-stoichiometric $\text{MgD}_{2-\eta}$ phase and $\text{TiD}_{2-\eta}$ phase, as well as the coherent interface between TiD_2 and Mg/ MgD_2 phases. As shown in Figure 12a, XRD can clearly characterize the phase composition of the composite material but struggles to distinguish its crystal structure. Therefore, neutron diffraction becomes crucial for analysis. In Figure 12b, the signal intensity of $\gamma\text{-MgD}_2$ is significantly stronger than in the XRD results. The combination of these results confirms the coexistence of both $\beta\text{-MgD}_2$ and $\gamma\text{-MgD}_2$ phases in the composite material. It is worth noting that, in neutron scattering analysis, different hydrogen isotopes may occupy different interstitial sites within the metal lattice and have varying activation diffusion barriers, which could impact the performance analysis of hydrogen storage materials. Thus, ensuring the accuracy of the research is another challenge that must be addressed when using this method in hydrogen storage material studies.

Neutron diffraction provides detailed information about the crystal structure, phase composition, and hydrogen occupancy in storage materials [108–110]. Inelastic neutron scattering, on the other hand, probes the vibrational and rotational dynamics of hydrogen within the material [111]. To harness the full potential of neutron scattering techniques, researchers have developed advanced instrumentation and data analysis methods [106]. The use of high-intensity neutron sources and optimized sample environments has enhanced the capabilities of these techniques [112]. Combining neutron scattering with complementary characterization methods, such as XRD and Raman spectroscopy, provides a comprehensive understanding of the structural and dynamic aspects of hydrogen storage materials.

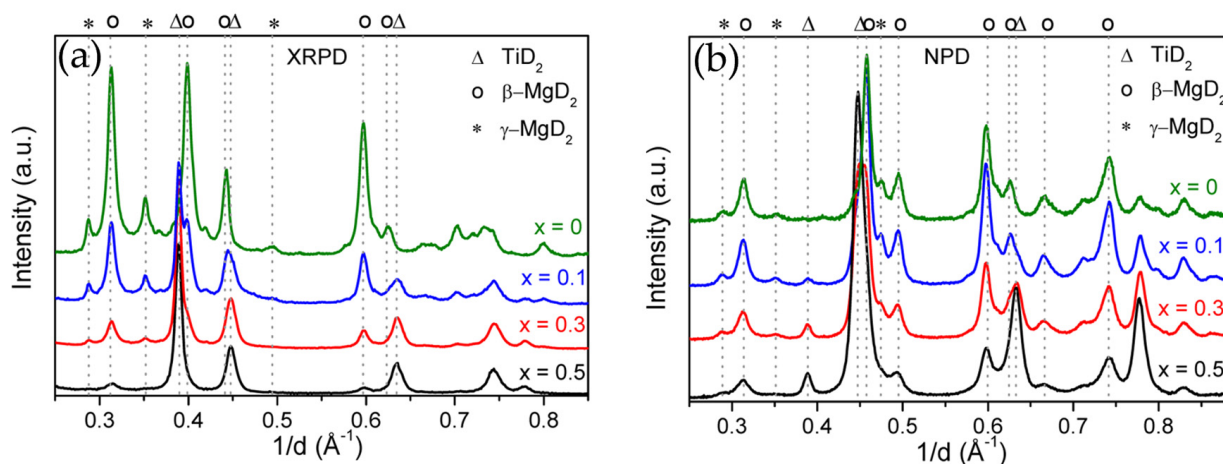


Figure 12. (a) X-ray and (b) neutron diffraction patterns of deuterated $(1-x)\text{MgD}_2-x\text{TiD}_2$ nanocomposites for $x = 0, 0.1, 0.3$, and 0.5 [107].

3.1.3. X-Ray Photoelectron Spectroscopy

X-ray photoelectron spectroscopy (XPS) is a surface-sensitive technique that provides valuable information about the elemental composition, chemical states, and electronic structure of hydrogen storage materials [113]. This method is based on the excitation of photoelectrons from a sample by X-rays and the measurement of the photoelectrons' kinetic energy to determine the elemental composition and chemical states of the sample. When X-rays illuminate a sample, the atoms in the sample absorb the X-ray energy and emit

photoelectrons (Figure 13). The kinetic energy of these photoelectrons is related to the energy of the incident X-rays and the binding energy of the atomic nucleus. By analyzing the photoelectron spectrum, one can obtain binding energy information for the elements on the sample surface, thereby determining the sample's elemental composition and chemical state [114].

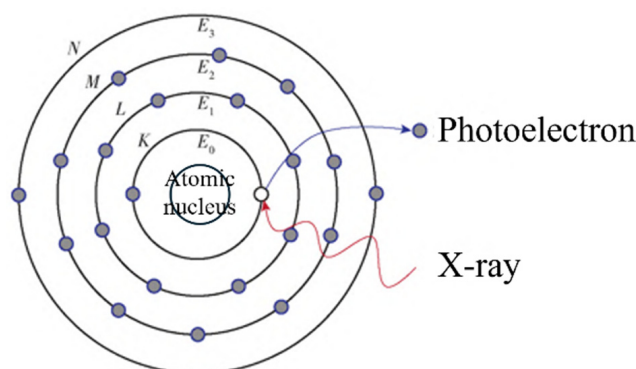


Figure 13. Schematic diagram of the XPS principle. E is the binding energy [113].

XPS is particularly useful for studying the surface chemistry of hydrogen storage materials, as it can probe the top few nanometers of the sample [115]. It can provide insights into the surface oxidation states, contamination levels, and chemical bonding between hydrogen and the host material [116,117]. XPS has been widely used to investigate the surface properties of metal hydrides, complex hydrides, and nanostructured storage materials [118,119].

Selvam et al. [120] utilized XPS to analyze Mg_2Cu and Mg_2Ni alloys exposed to air, finding that they undergo surface decomposition and preferential segregation of magnesium in the presence of oxygen and moisture. The segregated magnesium primarily existed as oxides and hydroxides on the surface, while Ni or Cu also appeared in oxidized states. The passivation of the alloys was caused by the oxidation of the transition metal components, and the researchers believed that the activation of these alloys involved the reduction of the oxidized three-dimensional elements and the formation of metal clusters. To investigate the influence of TiO_x on MgH_2 in greater depth, Zhang et al. [123] analyzed the internal chemical states of the samples using X-ray photoelectron spectroscopy (XPS). As shown in Figure 14a,b, compared to the single Ti^{4+} state in TiO_2 , the Ti in the $\text{Ni}_{0.034}\text{@TiO}_2$ catalyst exhibits a mixed valence state of Ti^{4+} and Ti^{3+} . During the dehydrogenation process, the content of Ti^{4+} and Ti^{3+} decreases, while the proportion of Ti^{2+} and Ti^0 increases. Meanwhile, due to the electronegativity of Ti (1.54), which lies between that of Mg (1.31) and H (2.20), it helps to weaken the Mg-H bond, thereby accelerating the dehydrogenation reaction. Throughout the evolution of Ti valence states, the valence state of oxygen (O) also changes. The O 1s XPS spectra of TiO_2 show two peaks located at 529.18 eV and 530.98 eV, corresponding to the Ti-O-Ti oxygen lattice (OL) and oxygen vacancies (OVs), respectively. The OL/OV ratio in TiO_2 is 87/13, while the OL/OV ratio in the $\text{Ni}_{0.034}\text{@TiO}_2$ catalyst is 71/29, significantly lower than that of TiO_2 . This indicates that the presence of single-atom Ni promotes the formation of oxygen vacancies. Additionally, the OL/OV ratio in the $\text{Ni}_x\text{@TiO}_2$ sample is also lower than that in TiO_2 , further proving that Ni facilitates the generation of oxygen vacancies. Combined with X-ray absorption spectroscopy data, the Ni in the $\text{Ni}_{0.034}\text{@TiO}_2$ catalyst exhibits a mixed positive valence state, with a strong electron-accepting capability. In this case, Ni attracts O ions, promoting the formation of oxygen vacancies in TiO_2 , resulting in a higher number of oxygen vacancies compared to that of pure TiO_2 . This is also consistent with recent findings on the influence of metal particles on oxygen vacancies. Figure 14c illustrates the catalytic mechanism during hydrogenation and dehydrogenation. Single-atom Ni can promote the formation of OVs and multivalent Ti^{x+} species around TiO_2 units. Oxygen vacancies serve as active sites that accelerate electron

transfer, while Ti^{x+} facilitates transitions between valence states via electron mediation, thus avoiding the high energy required to directly break the Mg-H bond. The atomic interface formed between isolated Ni atoms and Ti^{x+} constitutes dispersed Ni-O- Ti^{x+} active centers, thereby enhancing catalytic performance. Overall, the synergistic interaction between single-atom Ni and the TiO_2 support significantly improves the catalytic effect.

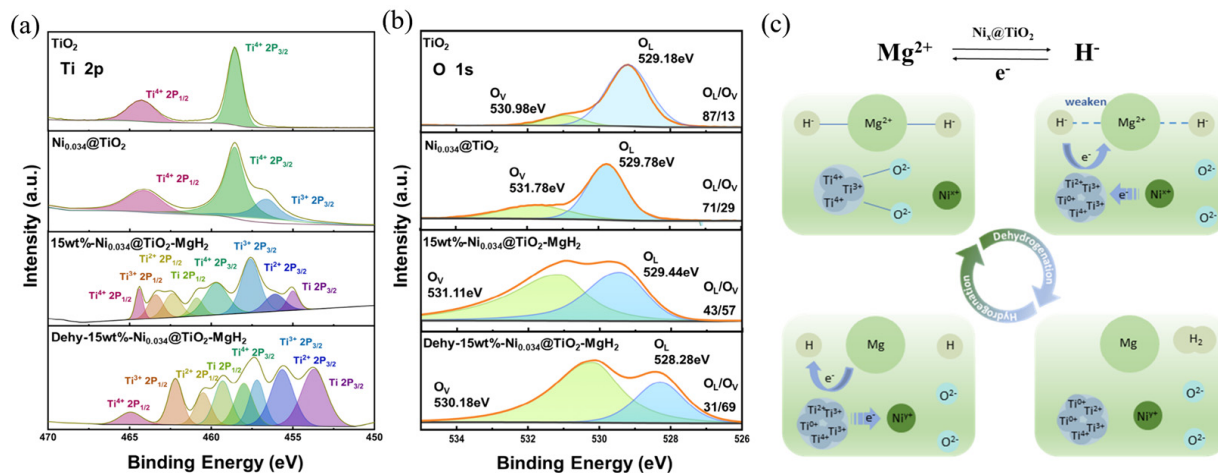


Figure 14. High-resolution XPS spectra of (a) Ti 2p and (b) O 1s, as well as (c) valence changes during the hydrogenation and dehydrogenation processes.

One of the key applications of XPS in hydrogen storage research is the study of surface catalysts and coatings that enhance the hydrogen sorption kinetics [121,122]. By analyzing the chemical composition and oxidation states of the surface species, the role of catalysts in promoting hydrogen dissociation, diffusion, and recombination can be elucidated. To overcome the limitations of XPS, researchers have developed advanced instrumentation and data analysis methods, such as synchrotron-based XPS for high-resolution measurements and in situ XPS studies for real-time monitoring of surface chemical changes. Combining XPS with other surface characterization techniques, such as scanning tunneling microscopy (STM) and atomic force microscopy (AFM), has provided a comprehensive understanding of the surface morphology and chemical properties of hydrogen storage materials. XPS has been crucial in understanding surface phenomena in hydrogen storage materials, particularly catalytic effects and degradation mechanisms.

3.2. Structure Characterization Techniques

3.2.1. Scanning Electron Microscopy

Scanning electron microscopy (SEM) is an ideal tool for studying the microstructure and surface characteristics of hydrogen storage materials due to its high-resolution imaging capabilities [125]. SEM can reveal detailed morphological features of materials, helping scientists understand the interactions between hydrogen and these materials, which is crucial for designing more efficient hydrogen storage systems [126,127]. The microstructure of materials, such as pore size, distribution, and surface roughness, directly affects the adsorption and diffusion rates of hydrogen.

Through SEM, researchers can clearly see these structural features and evaluate their specific impact on hydrogen storage performance. For example, larger pores may promote rapid hydrogen diffusion, while higher surface roughness can increase the surface area, providing more active sites for hydrogen adsorption. Additionally, SEM analysis can reveal potential defects on material surfaces, such as cracks, fractures, or other irregular shapes, which could affect the long-term stability and hydrogen storage efficiency of the materials. By regularly using SEM to monitor these materials, scientists can track performance changes during long-term use and adjust preparation processes or select more suitable materials accordingly. Silva et al. [124] used SEM to observe the surface morphology of

$\text{Ti}_{11}\text{V}_{30}\text{Nb}_{28}\text{Cr}_{31}$ at different stages of hydrogenation, finding that during laser processing, the surface of the debris particles melted, increasing the proportion of oxides near the surface. The manual grinding process leads to random particle size distribution, as shown in Figure 15a,d,g,j. Figure 15b,c illustrate that the surface of the particles after breaking the original alloy remains smooth with sharp edges, consistent with the brittle characteristics of the alloy. Figure 15e,f show that laser treatment significantly alters the particle surface, where rounded edges and a smooth surface suggest that the particles underwent remelting and rapid solidification. The inset in Figure 15f reveals microcracks on the remelted surface, which may contribute to the activation of the sample. Additionally, the remelted surface could restore the hydrogenation ability of the aged sample. Figure 15h,i,k,l display the similar behavior of both original and aged samples during hydrogenation. Surface cracks caused by volume expansion during the hydrogenation process were observed in particles analyzed under both conditions. These changes enhanced the alloy's hydrogen storage capacity. Therefore, surface remelting, oxide layer formation, and crack formation were confirmed to be factors influencing the hydrogen storage capacity of the pulse laser-activated $\text{Ti}_{11}\text{V}_{30}\text{Nb}_{28}\text{Cr}_{31}$ alloy.

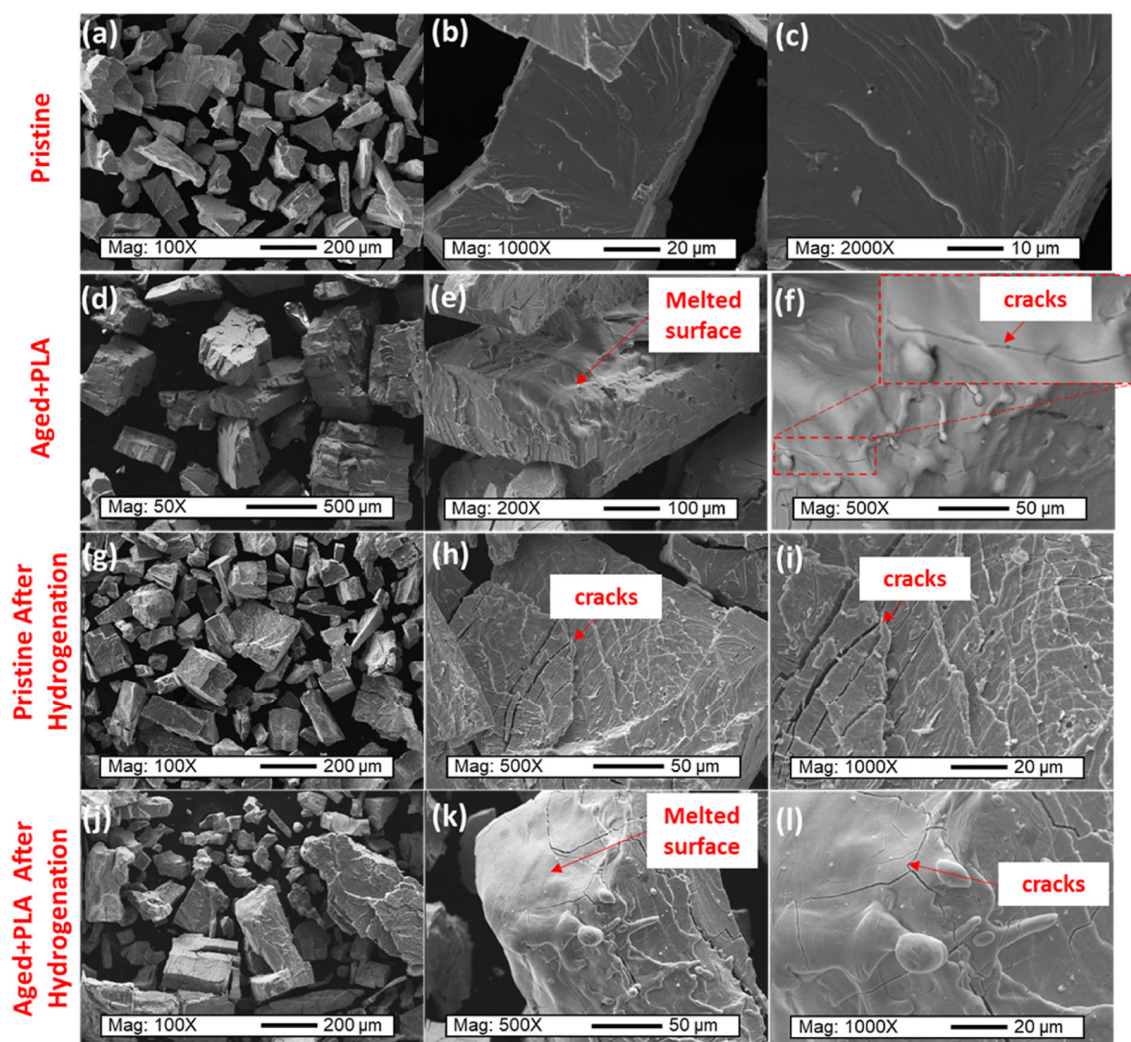


Figure 15. SEM analyses of the (a–c) pristine sample, (d–f) aged + PLA sample, (g–i) pristine sample after hydrogenation, and (j–l) aged + PLA sample after hydrogenation [124].

In recent years, the development of environmental scanning electron microscopy (ESEM) has brought revolutionary advancements to hydrogen storage research [128,131]. Unlike traditional SEM, ESEM allows for sample observation under near-natural conditions

without requiring high vacuum or complex sample preparation [130,132]. This enables researchers to directly monitor and record changes in material surfaces and microstructures during hydrogen absorption and desorption processes in real time. ESEM is particularly suitable for studying the interactions between hydrogen and materials. During hydrogen absorption, ESEM can capture morphological changes on the material surface, such as surface expansion, crack formation, or other structural deformations, in real time. These observations provide valuable information for optimizing material design and improving reaction speed and hydrogen storage capacity. Similarly, during hydrogen release, ESEM can offer crucial visual evidence to help scientists understand the material's regeneration capability and long-term stability.

3.2.2. Transmission and Scanning Transmission Electron Microscopy

Advanced electron microscopy techniques, particularly transmission electron microscopy (TEM), have revolutionized our understanding of hydrogen storage materials at the atomic scale [140]. With its superior resolution and accuracy, TEM allows researchers to observe the atomic and molecular structure of materials in unprecedented detail. This unique perspective provides scientists with critical insights into how these materials behave during hydrogen storage [142].

Through TEM, scientists can directly observe the atomic arrangement and molecular configuration within materials [141]. This capability not only helps reveal the fundamental structural characteristics of materials but also allows researchers to see subtle changes in the internal structure during hydrogen adsorption and desorption [143]. For example, researchers can observe how hydrogen atoms bond with specific sites within the material or how the lattice structure of the material deforms during hydrogen absorption. These detailed observations provide valuable information for understanding the behavior of hydrogen storage materials. By analyzing these microstructural changes, scientists can better comprehend the mechanisms of hydrogen adsorption and the key factors influencing storage capacity and release rate [149]. This in-depth understanding aids in developing new materials and optimizing the chemical composition and microstructure of existing materials to enhance their hydrogen storage performance. Furthermore, TEM's high-resolution imaging allows researchers to identify small defects within materials, such as dislocations, vacancies, and interfacial mismatches. These defects significantly impact the overall performance of materials, especially during repeated cycles of hydrogen adsorption and desorption. Therefore, accurately identifying and analyzing these defects is crucial for designing more durable and efficient hydrogen storage materials. Wu et al. [150] prepared LiBH_4 composites confined within bilayer carbon nanobowls through a strong capillary effect under 100 bar H_2 pressure. TEM analysis confirmed the gradual formation of bilayer carbon nanobowls. Benefiting from the nanoscale confinement and catalytic functions of carbon, the composite released hydrogen from 225 °C, peaking at 353 °C, with a hydrogen release amount of up to 10.9 wt.%. Compared to bulk LiBH_4 , the peak dehydrogenation temperature decreased by 112 °C. More importantly, the composite absorbed about 8.5 wt.% H_2 at 300 °C and 100 bar H_2 , demonstrating significant reversible hydrogen storage capability. Ren et al. [133] investigated the dehydrogenation mechanism of the $\text{MgH}_2/\text{Ni@pCNF}$ composite using in situ high-resolution transmission electron microscopy (HRTEM) to observe the microstructural evolution under electron-beam irradiation. Figure 16a–c show HAADF, BF, and corresponding element mapping images of hydrogenated $\text{MgH}_2/\text{Ni@pCNF}$, with the red dashed box indicating the irradiated area. Figure 16d–g present the HRTEM images of the composite material during the hydrogen release process, where the lattice fringes observed in the selected area electron-diffraction patterns in each subfigure correspond to the phase changes of the material throughout the reaction. Before irradiation, lattice fringes were used to identify MgH_2 (101) (Figure 16(d1)), Mg_2NiH_4 (311) (Figure 16(d2)), and MgO (200) (Figure 16(d3)). Additionally, amorphous carbon frameworks of pCNF, acting as scaffolds for the nanoconfined MgH_2 , were observed in all HRTEM images (Figure 16d–g). After 3 min of irradiation, part of the Mg_2NiH_4 began to decompose, converting into Mg_2Ni

(Figure 16(e2)). A 0.246 nm plane spacing was observed between MgH_2 (Figure 16(e3)) and Mg_2NiH_4 (Figure 16(e4)), corresponding to Mg (101) (Figure 16(e1)), indicating that MgH_2 near Mg_2NiH_4 was also starting to decompose. The desorption of Mg_2NiH_4 induced lattice volume changes, which introduced internal stress and defects at the $\text{Mg}_2\text{NiH}_4/\text{MgH}_2$ interface, promoting MgH_2 desorption. Furthermore, the interface between the catalyst ($\text{Mg}_2\text{NiH}_4/\text{Mg}_2\text{Ni}$) and the matrix (MgH_2) facilitated rapid hydrogen diffusion, accelerating MgH_2 desorption. After 6 min of irradiation, only Mg_2Ni (Figure 16(f2)), Mg (Figure 16(f1)), and MgH_2 (Figure 16(f3)) remained, indicating that Mg_2NiH_4 completely decomposed earlier than MgH_2 . After 10 min of electron-beam irradiation, the hydrogen in the irradiated area was fully released and transferred to Mg (Figure 15(g1)) and Mg_2Ni (Figure 15(g2)). Moreover, due to the confinement of pCNF, the Mg -based nanoparticles did not experience significant growth or agglomeration.

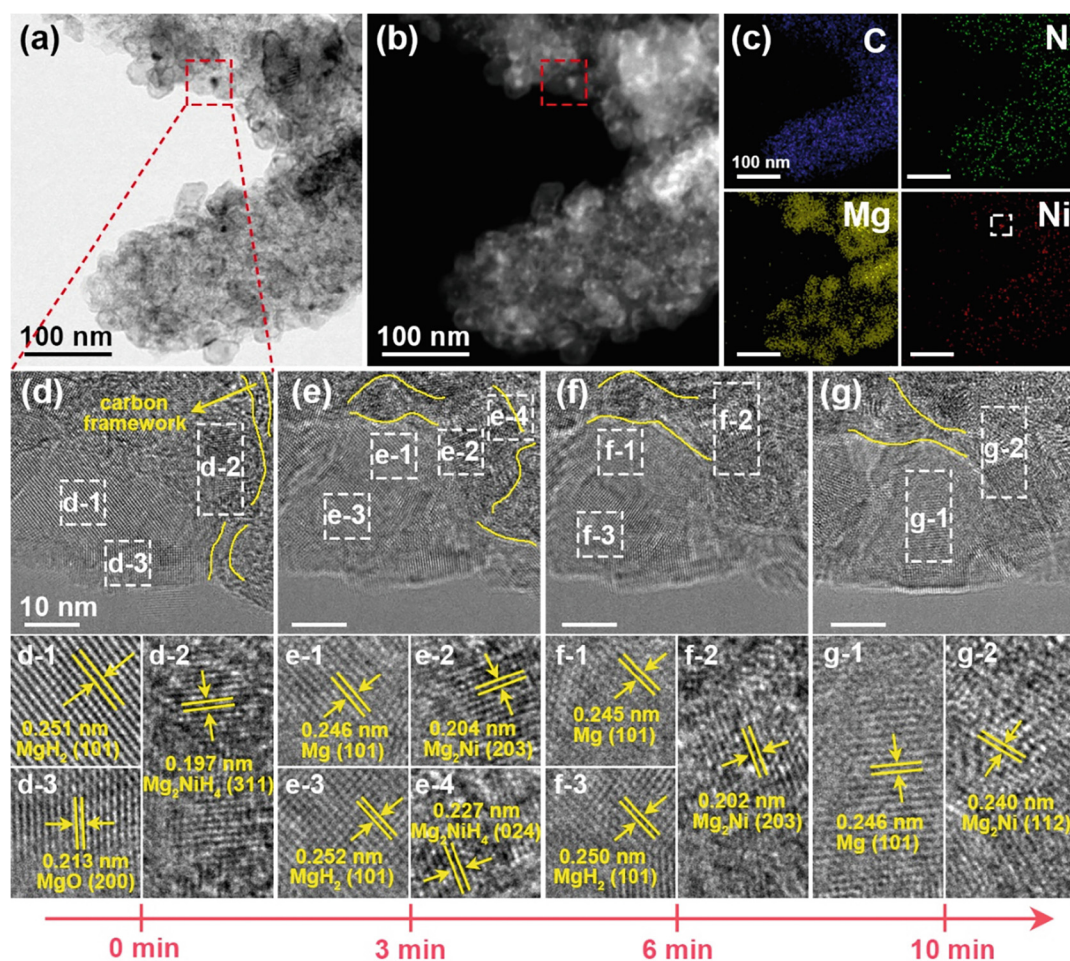


Figure 16. In situ TEM analysis of the hydrogenated $\text{MgH}_2/\text{Ni}@p\text{CNF}$ composites: (a) HAADF image (the square marked by red dotted line indicates the irradiated area). (b) BF image. (c) The corresponding elemental mapping of C, N, Mg, and Ni. (d–g) HRTEM images and selective electron diffraction at random points showing the evolution of microstructure upon hydrogen desorption induced by the electron-beam irradiation. (d1–d3) Initial microstructure showing lattice fringes of MgH_2 (101), Mg_2NiH_4 (311), and MgO (200), respectively, before irradiation. (e1–e4) After 3 min, partial decomposition of Mg_2NiH_4 into Mg_2Ni begins, with defects forming at the $\text{Mg}_2\text{NiH}_4/\text{MgH}_2$ interface, promoting hydrogen desorption, while some MgH_2 remains stable. (f1–f3) At 6 min, complete decomposition of Mg_2NiH_4 is observed, while MgH_2 remains partially stable, and Mg nanoparticles become visible. (g1,g2) After 10 min, hydrogen is fully released and transferred to Mg and Mg_2Ni [133].

Additionally, the development of in situ environmental transmission electron microscopy (E-TEM) has made it possible to observe materials directly under dynamic, real-world conditions, which is crucial for studying hydrogen storage materials [147,148]. Traditional TEM requires vacuum conditions, limiting the observation of material behavior under actual operating conditions [145,146]. In contrast, E-TEM allows for the observation of materials in a gaseous environment, which can include hydrogen, thus providing genuine insights into the behavior of these materials during hydrogen adsorption and desorption [144]. Through E-TEM, researchers can observe structural changes during the hydrogen cycling process in real time [151,152]. This includes observing how atoms rearrange, how defects in the material evolve, and how the crystal structure of the material changes during hydrogen adsorption and release. These observations are critical for understanding the mechanisms of hydrogen adsorption and the factors influencing the efficiency and durability of storage materials. Future rational use of E-TEM can help identify the best materials and designs for hydrogen storage, allowing scientists to conduct experiments on different materials and under various environmental conditions.

3.2.3. Atomic Force Microscopy

Atomic force microscopy (AFM), as a precise surface analysis tool, has provided valuable insights into the surface morphology and mechanical properties of hydrogen storage materials [135,137]. AFM measures forces through interactions between the probe and the sample surface, allowing for nanoscale mapping of material surfaces [136,138]. This detailed surface characterization is crucial for understanding and optimizing the performance of hydrogen storage materials [134]. AFM's high-resolution imaging capabilities enable it to reveal the microstructure of materials, such as nanoparticles, pores, and cracks, which are key factors in evaluating the adsorption capacity of materials. Furthermore, AFM can measure mechanical properties such as hardness and elastic modulus, which are critical for designing hydrogen storage systems that maintain structural stability under various operating conditions.

Kalisvaart et al. [139] used AFM to analyze the surface changes of Mg and Mg-10%Cr-10%V films in both deposited and hydrogenated states. As shown in Figure 17, the surface of the deposited palladium (Pd) film is extremely smooth, with a root-mean-square (RMS) roughness of only 5 Å. In the hydrogenated state, the Pd layer appears to break into small particles with diameters of approximately 20 nm, leading to a 2- to 13-fold increase in the measured RMS roughness. Due to the tip effect, atomic force microscopy (AFM) often underestimates roughness. In fact, because of the close spacing of Pd particles, the relatively large tip radius of the AFM (6 nm) almost certainly leads to a significant underestimation of roughness, especially in hydrogenated samples. Therefore, the increase in surface roughness observed after combining neutron reflectometry (NR) data are primarily attributed to the fragmentation of the Pd layer into small particles.

Recent advancements in high-speed atomic force microscopy (high-speed AFM) technology have enabled scientists to observe dynamic processes at the nanoscale in real time [153,154]. High-speed AFM significantly improves imaging speed, allowing researchers to observe and record changes in material surfaces during hydrogen adsorption and desorption almost in real time [155,156]. This capability is particularly important for understanding the dynamic characteristics of hydrogen–material interactions [157]. For example, through high-speed AFM, researchers can directly observe changes in surface morphology caused by hydrogen adsorption, such as slight expansion or contraction of the surface. These changes might be difficult to capture with traditional AFM due to their rapid occurrence. Additionally, this technology can be used to study the fatigue behavior of materials during multiple cycles of hydrogen adsorption and desorption, providing direct experimental data for assessing the long-term stability and reusability of materials.

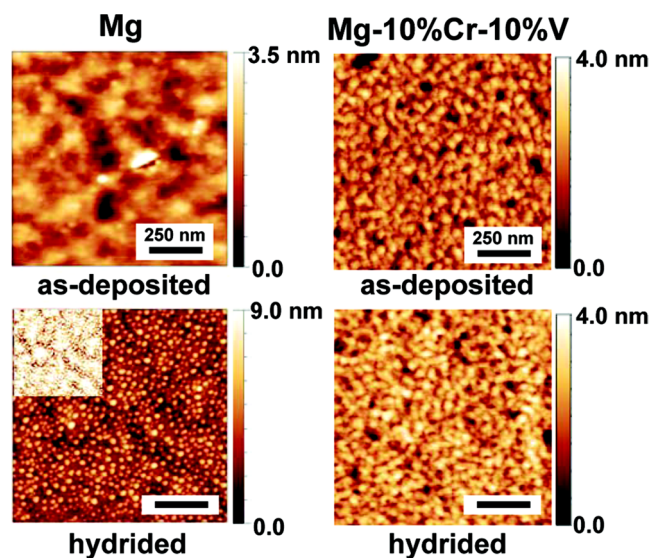


Figure 17. AFM micrographs of Ta/Mg/CrV/Pd and Ta/Mg-10%Cr-10%V/CrV/Pd in the as-deposited and hydrogenated state. The Ta/Mg/CrV/Pd was hydrogenated at 50 mbar for 14 h and Ta/Mg-10%Cr-10%V/CrV/Pd at 10 mbar for 20 h. The inset shows the micrograph of the hydrided film on the same brightness scale as the as-deposited state for Ta/Mg/CrV/Pd [139].

4. Challenges and Limitations

4.1. Obstacles and Limitations in Hydrogen Storage Performance Characterization

The characterization of hydrogen storage performance faces multifaceted challenges that significantly impact the accuracy, reliability, and interpretability of experimental data.

Volumetric measurements, particularly the Sieverts method, are susceptible to systematic errors arising from thermal gradients, pressure sensor drift, and gas impurities. Zhou et al. [21] highlighted the critical impact of temperature gradients on volumetric measurements, demonstrating how even minor thermal fluctuations can lead to substantial errors in calculated hydrogen uptake. This issue is particularly pronounced for materials with low storage capacities or slow kinetics, where small measurement errors can lead to significant overestimation or underestimation of storage performance.

The challenge of achieving true equilibrium conditions during measurements is exacerbated by the slow kinetics of many advanced storage materials. Complex hydrides and nanostructured composites often exhibit multi-step absorption/desorption processes with varying time scales, making it difficult to determine when true equilibrium has been reached. This kinetic limitation can lead to underestimation of storage capacities and misinterpretation of thermodynamic parameters, particularly when fixed measurement times are used across different materials.

The discrepancy between laboratory-scale measurements and real-world performance remains a significant hurdle. Factors such as heat and mass transfer limitations, which are often negligible in small-scale experiments, become critical in larger systems. The work of Ding et al. [28] on nanostructured $\text{LiBH}_4\text{-MgH}_2$ systems exemplifies this challenge, where the excellent performance observed in laboratory tests may not directly translate to practical storage systems due to scaling effects on heat transfer and reaction kinetics.

4.2. Challenges and Constraints in Structure and Composition Characterization

The structural and compositional characterization of hydrogen storage materials presents unique challenges that limit our ability to fully understand storage mechanisms and material properties.

In situ characterization, which observes materials in their “native environment”, and operando characterization, which captures real-time data under “actual working conditions”, can provide researchers with deep insights into the structural and functional

changes of materials. Although in situ and operando characterization techniques are highly powerful, they often require certain compromises in experimental conditions, such as reduced resolution, decreased sensitivity, or simplified setups, to meet the demands of real-time monitoring. In situ TEM, for instance, allows real-time observation of structural changes during hydrogen absorption/desorption but typically operates at lower pressures than those used in practical storage systems. This pressure gap can lead to observations that may not accurately represent material behavior under realistic conditions. The study by Ren et al. [133] on $\text{MgH}_2/\text{Ni@pCNF}$ composites using in situ HRTEM illustrates both the power and limitations of these techniques in studying the dehydrogenation mechanism of complex nanostructured materials.

Raman spectroscopy, while sensitive to hydrogen-containing bonds, faces challenges in quantitative analysis due to variations in scattering cross-sections and the potential for laser-induced sample heating. The work of Pedraza et al. [82] on ammonia borane decomposition demonstrates both the power and limitations of Raman spectroscopy in studying hydrogen storage materials, highlighting the need for careful experimental design and data interpretation.

The characterization of multi-component and nanostructured materials presents additional complexities. Techniques like XPS and SIMS offer high surface sensitivity but may not accurately represent bulk compositions. Conversely, bulk techniques may overlook critical surface phenomena that govern hydrogen uptake and release. The study by Xing et al. [121] on carbon-coated CoNi nanocatalysts illustrates the challenge of characterizing complex nanostructured materials, where the distribution and chemical state of catalytic components play crucial roles in enhancing storage performance.

Addressing these challenges requires continued development of advanced characterization tools, improved experimental protocols, and sophisticated data analysis methods. Emerging approaches, such as machine learning-assisted data interpretation and multi-modal characterization platforms [158], offer promising avenues for overcoming current limitations. However, realizing the full potential of these advanced characterization approaches will require close collaboration between experimentalists, theorists, and instrument developers to ensure that the data obtained accurately reflects the intrinsic properties and behavior of hydrogen storage materials under realistic operating conditions.

5. Conclusions and Perspective

The field of solid-state hydrogen storage materials has made significant strides in recent years, with the development of advanced characterization techniques and the emergence of novel materials. However, ongoing challenges in understanding the complex hydrogen storage mechanisms and optimizing material performance necessitate continued research and innovation.

This comprehensive review has provided an overview of the key characterization techniques employed in the field of solid-state hydrogen storage, discussing their principles, advantages, limitations, and synergistic applications. Conventional techniques such as Sieverts method, gravimetric analysis, SIMS, TDS, neutron scattering, and electrochemical methods have been discussed in detail, highlighting their roles in unraveling the intricate relationship between the structure, composition, and properties of hydrogen storage materials. Emerging optical characterization techniques, including Raman spectroscopy, XRD, and XPS, have been explored, emphasizing their potential in providing insights into the local structure, bonding, and surface chemistry of these materials.

Practical considerations, such as equipment availability, sample preparation, and cost-effectiveness, have been addressed to provide a pragmatic guide for researchers in the field. The challenges associated with characterizing novel hydrogen storage materials, such as nanoconfined hydrides, MOFs, and graphene-related materials, have been highlighted, and innovative approaches to tackle these challenges have been discussed.

Looking ahead, the integration of in situ and operando characterization techniques, computational modeling, and data-driven approaches will be crucial for accelerating the

discovery and optimization of high-performance hydrogen storage materials. Collaborative efforts among researchers from diverse disciplines and the establishment of standardized characterization protocols and databases will be essential for advancing the field towards practical applications.

As the world transitions towards a sustainable energy future, the development of efficient and reliable hydrogen storage solutions will play a critical role in enabling the widespread adoption of clean energy technologies. By addressing the characterization challenges and embracing innovative approaches, the scientific community can unlock the full potential of solid-state hydrogen storage materials and contribute to the realization of a hydrogen-based energy economy.

Funding: This study was financially supported by the Opening Project of Crystalline Silicon Photovoltaic New Energy Research Institute (2022CHXK002), and the Leshan Normal University Research Program (KYPY2023-0001).

Conflicts of Interest: The authors declare no conflicts of interest.

References

- Cheng, H.; Chen, L.; Cooper, A.C.; Sha, X.; Pez, G.P. Hydrogen spillover in the context of hydrogen storage using solid-state materials. *Energy Environ. Sci.* **2008**, *1*, 338–354. [\[CrossRef\]](#)
- Broom, D.P.; Hirscher, M. Irreproducibility in hydrogen storage material research. *Energy Environ. Sci.* **2016**, *9*, 3368–3380. [\[CrossRef\]](#)
- Gupta, A.; Baron, G.V.; Perreault, P.; Lenaerts, S.; Ciocarlan, R.-G.; Cool, P.; Mileo, P.G.M.; Rogge, S.; Van Speybroeck, V.; Watson, G.; et al. Hydrogen Clathrates: Next Generation Hydrogen Storage Materials. *Energy Storage Mater.* **2021**, *41*, 69–107. [\[CrossRef\]](#)
- Cho, E.S.; Ruminski, A.M.; Liu, Y.S.; Shea, P.T.; Kang, S.; Zaia, E.W.; Park, J.Y.; Chuang, Y.D.; Yuk, J.M.; Zhou, X.; et al. Hierarchically Controlled Inside-Out Doping of Mg Nanocomposites for Moderate Temperature Hydrogen Storage. *Adv. Funct. Mater.* **2017**, *27*, 1704316. [\[CrossRef\]](#)
- Wang, Y.; Xue, Y.; Züttel, A. Nanoscale engineering of solid-state materials for boosting hydrogen storage. *Chem. Soc. Rev.* **2024**, *53*, 972–1003. [\[CrossRef\]](#)
- Schneemann, A.; White, J.L.; Kang, S.; Jeong, S.; Wan, L.F.; Cho, E.S.; Heo, T.W.; Prendergast, D.; Urban, J.J.; Wood, B.C.; et al. Nanostructured Metal Hydrides for Hydrogen Storage. *Chem. Rev.* **2018**, *118*, 10775–10839. [\[CrossRef\]](#)
- Gao, Y.; Li, Z.; Wang, P.; Li, C.; Yue, Q.; Cui, W.G.; Wang, X.; Yang, Y.; Gao, F.; Zhang, M.; et al. Solid-State Hydrogen Storage Origin and Design Principles of Carbon-Based Light Metal Single-Atom Materials. *Adv. Funct. Mater.* **2024**, *34*, 2316368. [\[CrossRef\]](#)
- Li, Y.; Guo, Q.; Ding, Z.; Jiang, H.; Yang, H.; Du, W.; Zheng, Y.; Huo, K.; Shaw, L.L. MOFs-Based Materials for Solid-State Hydrogen Storage: Strategies and Perspectives. *Chem. Eng. J.* **2024**, *485*, 149665. [\[CrossRef\]](#)
- Allendorf, M.D.; Hulvey, Z.; Gennett, T.; Ahmed, A.; Autrey, T.; Camp, J.; Seon Cho, E.; Furukawa, H.; Haranczyk, M.; Head-Gordon, M.; et al. An assessment of strategies for the development of solid-state adsorbents for vehicular hydrogen storage. *Energy Environ. Sci.* **2018**, *11*, 2784–2812. [\[CrossRef\]](#)
- Wei, T.Y.; Lim, K.L.; Tseng, Y.S.; Chan, S.L.I. A review on the characterization of hydrogen in hydrogen storage materials. *Renew. Sustain. Energy Rev.* **2017**, *79*, 1122–1133. [\[CrossRef\]](#)
- Sun, C.; Wang, C.; Ha, T.; Lee, J.; Shim, J.H.; Kim, Y. A brief review of characterization techniques with different length scales for hydrogen storage materials. *Nano Energy* **2023**, *113*, 108554. [\[CrossRef\]](#)
- Afanasev, A.V.; Karlovets, D.V.; Serbo, V.G. Elastic scattering of twisted neutrons by nuclei. *Phys. Rev. C* **2021**, *103*, 054612. [\[CrossRef\]](#)
- Aguilar, V.; Ruvalcaba-Sil, J.L.; Bucio, L.; Rivera-Muñoz, E.M. Characterization and setting protocol for a simultaneous X-ray Diffraction-X-ray Fluorescence system (XRD/XRF) for in situ analysis. *Eur. Phys. J. Plus* **2019**, *134*, 286. [\[CrossRef\]](#)
- Hannon, A.C.; Gibbs, A.S.; Takagi, H. Neutron scattering length determination by means of total scattering. *J. Appl. Crystallogr.* **2018**, *51*, 854–866. [\[CrossRef\]](#)
- Korolkovas, A. Fast X-ray diffraction (XRD) tomography for enhanced identification of materials. *Sci. Rep.* **2022**, *12*, 19097. [\[CrossRef\]](#)
- Kumar, P.; Singh, S.; Hashmi, S.A.R.; Kim, K.-H. MXenes: Emerging 2D materials for hydrogen storage. *Nano Energy* **2021**, *85*, 105989. [\[CrossRef\]](#)
- Tan, W.L.; McNeill, C.R. X-ray diffraction of photovoltaic perovskites: Principles and applications. *Appl. Phys. Rev.* **2022**, *9*, 021310. [\[CrossRef\]](#)
- Xia, Y.; Yang, Z.; Zhu, Y. Porous carbon-based materials for hydrogen storage: Advancement and challenges. *J. Mater. Chem. A* **2013**, *1*, 9365–9381. [\[CrossRef\]](#)
- Kittner, N.; Lill, F.; Kammen, D.M. Energy storage deployment and innovation for the clean energy transition. *Nat. Energy* **2017**, *2*, 17125. [\[CrossRef\]](#)

20. Gao, Y.; Li, Z.; Wang, P.; Cui, W.G.; Wang, X.; Yang, Y.; Gao, F.; Zhang, M.; Gan, J.; Li, C.; et al. Experimentally validated design principles of heteroatom-doped-graphene-supported calcium single-atom materials for non-dissociative chemisorption solid-state hydrogen storage. *Nat. Commun.* **2024**, *15*, 928. [\[CrossRef\]](#)
21. Liu, Y.; Du, H.; Zhang, X.; Yang, Y.; Gao, M.; Pan, H. Superior catalytic activity derived from a two-dimensional Ti_3C_2 precursor towards the hydrogen storage reaction of magnesium hydride. *Chem. Commun.* **2016**, *52*, 705–708. [\[CrossRef\]](#) [\[PubMed\]](#)
22. Pan, H.; Liu, Y.; Gao, M.; Zhu, Y.; Lei, Y.; Wang, Q. An investigation on the structural and electrochemical properties of $\text{La}_{0.7}\text{Mg}_{0.3}(\text{Ni}_{0.85}\text{Co}_{0.15})_x$ ($x = 3.15 - 3.80$) hydrogen storage electrode alloys. *J. Alloys Compd.* **2003**, *351*, 228–234. [\[CrossRef\]](#)
23. Ding, Z.; Li, Y.; Jiang, H.; Zhou, Y.; Wan, H.; Qiu, J.; Jiang, F.; Tan, J.; Du, W.; Chen, Y.; et al. The integral role of high-entropy alloys in advancing solid-state hydrogen storage. *Interdiscip. Mater.* **2024**, 1–34. [\[CrossRef\]](#)
24. Liu, Y.; Pan, H.; Gao, M.; Wang, Q. Advanced hydrogen storage alloys for Ni/MH rechargeable batteries. *J. Mater. Chem.* **2011**, *21*, 4743–4755. [\[CrossRef\]](#)
25. Zhang, X.; Liu, Y.; Ren, Z.; Zhang, X.; Hu, J.; Huang, Z.; Lu, Y.; Gao, M.; Pan, H. Realizing 6.7 wt% reversible storage of hydrogen at ambient temperature with non-confined ultrafine magnesium hydrides. *Energy Environ. Sci.* **2021**, *14*, 2302–2313. [\[CrossRef\]](#)
26. Yang, H.; Ding, Z.; Li, Y.-T.; Li, S.-Y.; Wu, P.-K.; Hou, Q.-H.; Zheng, Y.; Gao, B.; Huo, K.-F.; Du, W.-J.; et al. Recent advances in kinetic and thermodynamic regulation of magnesium hydride for hydrogen storage. *Rare Met.* **2023**, *42*, 2906–2927. [\[CrossRef\]](#)
27. Ding, Z.; Li, H.; Yan, G.; Yang, W.; Gao, Z.; Ma, W.; Shaw, L. Mechanism of hydrogen storage on Fe_3B . *Chem. Commun.* **2020**, *56*, 14235–14238. [\[CrossRef\]](#)
28. Liu, Y.; Zhong, K.; Luo, K.; Gao, M.; Pan, H.; Wang, Q. Size-Dependent Kinetic Enhancement in Hydrogen Absorption and Desorption of the Li–Mg–N–H System. *J. Am. Chem. Soc.* **2009**, *131*, 1862–1870. [\[CrossRef\]](#)
29. Pang, Y.; Liu, Y.; Gao, M.; Ouyang, L.; Liu, J.; Wang, H.; Zhu, M.; Pan, H. A mechanical-force-driven physical vapour deposition approach to fabricating complex hydride nanostructures. *Nat. Commun.* **2014**, *5*, 3519. [\[CrossRef\]](#)
30. Ding, Z.; Li, Y.; Yang, H.; Lu, Y.; Tan, J.; Li, J.; Li, Q.; Chen, Y.a.; Shaw, L.L.; Pan, F. Tailoring MgH_2 for hydrogen storage through nanoengineering and catalysis. *J. Magnes. Alloys* **2022**, *10*, 2946–2967. [\[CrossRef\]](#)
31. Usman, M.R. Hydrogen storage methods: Review and current status. *Renew. Sustain. Energy Rev.* **2022**, *167*, 112743. [\[CrossRef\]](#)
32. Zhou, D.; Ye, Y.; Zhu, H.; Cheng, H. Thermal analysis and performance improvement of heat transfer in sample cell of Sieverts apparatus. *Int. J. Hydrog. Energy* **2024**, *50*, 61–70. [\[CrossRef\]](#)
33. Charbonnier, V.; Asano, K.; Kim, H.; Sakaki, K. How to evaluate hydrogen storage properties by Sieverts’ method in the pressure range up to 100 MPa. *J. Alloys Compd.* **2023**, *960*, 170860. [\[CrossRef\]](#)
34. Gray, E.M. 7-Reliably measuring hydrogen uptake in storage materials. In *Solid-State Hydrogen Storage*; Walker, G., Ed.; Woodhead Publishing: Cambridge, UK, 2008; pp. 174–204. [\[CrossRef\]](#)
35. Webb, C.J.; Gray, E.M. The effect of inaccurate volume calibrations on hydrogen uptake measured by the Sieverts method. *Int. J. Hydrog. Energy* **2014**, *39*, 2168–2174. [\[CrossRef\]](#)
36. Webb, C.J.; Gray, E.M. Analysis of the uncertainties in gas uptake measurements using the Sieverts method. *Int. J. Hydrog. Energy* **2014**, *39*, 366–375. [\[CrossRef\]](#)
37. Ding, Z.; Li, H.; Shaw, L. New insights into the solid-state hydrogen storage of nanostructured $\text{LiBH}_4\text{-MgH}_2$ system. *Chem. Eng. J.* **2020**, *385*, 123856. [\[CrossRef\]](#)
38. Zhu, H.; Zhou, D.; Chen, D.; Cheng, H. Design of ultra-efficient and automatically temperature-variable cycle (TVC) Sieverts apparatus for testing sorption properties of hydrogen storage materials. *Int. J. Hydrog. Energy* **2024**, *62*, 172–185. [\[CrossRef\]](#)
39. Kadono, J.; Maruoka, T.; Nakazawa, D.; Hoshiyama, Y.; Miyake, H. Measuring the effects of boron mass addition to V–Fe hydrogen storage alloys on their hydrogen absorbing–desorbing characteristics and loss of boron by hydrogenation by employing new analysis methods; hybrid of Sieverts’ method, inert gas fusion method, and gravimetric method. *Int. J. Hydrog. Energy* **2017**, *42*, 996–1003. [\[CrossRef\]](#)
40. Hurst, K.E.; Gennett, T.; Adams, J.; Allendorf, M.D.; Balderas-Xicohtencatl, R.; Bielewski, M.; Edwards, B.; Espinal, L.; Fultz, B.; Hirscher, M.; et al. An International Laboratory Comparison Study of Volumetric and Gravimetric Hydrogen Adsorption Measurements. *ChemPhysChem* **2019**, *20*, 1997–2009. [\[CrossRef\]](#)
41. Alomairy, S. Dissolution mechanism and kinetics of $\beta(\text{Mg17Al12})$ phases in AZ91 magnesium alloy. *J. Magnes. Alloys* **2024**, *12*, 1581–1592. [\[CrossRef\]](#)
42. Baird, J.A.; Taylor, L.S. Evaluation of amorphous solid dispersion properties using thermal analysis techniques. *Adv. Drug Deliv. Rev.* **2012**, *64*, 396–421. [\[CrossRef\]](#) [\[PubMed\]](#)
43. Demers, V.; Turenne, S.; Scalzo, O. Segregation measurement of powder injection molding feedstock using thermogravimetric analysis, pycnometer density and differential scanning calorimetry techniques. *Adv. Powder Technol.* **2015**, *26*, 997–1004. [\[CrossRef\]](#)
44. Drzeżdżon, J.; Jacewicz, D.; Sielicka, A.; Chmurzyński, L. Characterization of polymers based on differential scanning calorimetry based techniques. *TrAC Trends Anal. Chem.* **2019**, *110*, 51–56. [\[CrossRef\]](#)
45. Green, S.P.; Wheelhouse, K.M.; Payne, A.D.; Hallett, J.P.; Miller, P.W.; Bull, J.A. On the Use of Differential Scanning Calorimetry for Thermal Hazard Assessment of New Chemistry: Avoiding Explosive Mistakes. *Angew. Chem. Int. Ed.* **2020**, *59*, 15798–15802. [\[CrossRef\]](#)
46. Saadatkah, N.; Carillo Garcia, A.; Ackermann, S.; Leclerc, P.; Latifi, M.; Samih, S.; Patience, G.S.; Chaouki, J. Experimental methods in chemical engineering: Thermogravimetric analysis—TGA. *Can. J. Chem. Eng.* **2019**, *98*, 34–43. [\[CrossRef\]](#)

47. Sanchez-Ruiz, J.M. Probing free-energy surfaces with differential scanning calorimetry. *Annu. Rev. Phys. Chem.* **2011**, *62*, 231–255. [CrossRef]
48. Xiao, H.; Qian, F.; Zhang, X.; Hu, H.; Tang, R.; Hu, C.; Zhou, W.; He, X.; Pu, Z.; Ma, C.; et al. Effect of Ce_{0.6}Zr_{0.4}O₂ nanocrystals on boosting hydrogen storage performance of MgH₂. *Chem. Eng. J.* **2024**, *494*, 153203. [CrossRef]
49. Benninghoven, A.; Huber, A.M.; Werner, H.W. Secondary ion mass spectrometry (SIMS VI): Wiley, Chichester, 1988 (ISBN 0-471-91832-6). xxvii + 1078 pp. Price £75.00. *Anal. Chim. Acta* **1988**, *215*, 366. [CrossRef]
50. Benninghoven, A. Surface analysis by Secondary Ion Mass Spectrometry (SIMS). *Surf. Sci.* **1994**, *299*, 246–260. [CrossRef]
51. Lockyer, N.P.; Aoyagi, S.; Fletcher, J.S.; Gilmore, I.S.; van der Heide, P.A.W.; Moore, K.L.; Tyler, B.J.; Weng, L.-T. Secondary ion mass spectrometry. *Nat. Rev. Methods Primers* **2024**, *4*, 32. [CrossRef]
52. Madroñero, A.; Aguado, J.; Blanco, J.M.; López, A. Uptake of hydrogen from some carbon fibres examined by Secondary Ion Mass Spectrometry. *Appl. Surf. Sci.* **2011**, *257*, 1881–1885. [CrossRef]
53. Andersen, D.; Chen, H.; Pal, S.; Cressa, L.; De Castro, O.; Wirtz, T.; Schmitz, G.; Eswara, S. Correlative high-resolution imaging of hydrogen in Mg₂Ni hydrogen storage thin films. *Int. J. Hydrog. Energy* **2023**, *48*, 13943–13954. [CrossRef]
54. Hryniewicz, T.; Konarski, P.; Rokicki, R. Hydrogen Reduction in MEP Niobium Studied by Secondary Ion Mass Spectrometry (SIMS). *Metals* **2017**, *7*, 442. [CrossRef]
55. Lagator, M.; Berrueta Razo, I.; Royle, T.; Lockyer, N.P. Sensitivity enhancement using chemically reactive gas cluster ion beams in secondary ion mass spectrometry (SIMS). *Surf. Interface Anal.* **2022**, *54*, 349–355. [CrossRef]
56. Francois-Saint-Cyr, H.; Martin, I.; Peres, P.; Guillermier, C.; Prosa, T.; Blanc, W.; Larson, D. Secondary Ion Mass Spectrometry (SIMS) and Atom Probe Tomography (APT): Powerful Synergetic Techniques for Materials Scientists. *Microsc. Microanal.* **2020**, *26*, 524–525. [CrossRef]
57. Liu, Y.; Lorenz, M.; Ievlev, A.V.; Ovchinnikova, O.S. Secondary Ion Mass Spectrometry (SIMS) for Chemical Characterization of Metal Halide Perovskites. *Adv. Funct. Mater.* **2020**, *30*, 2002201. [CrossRef]
58. Gao, Y.-Y.; Ren, T.-X.; Williams, I.S.; Ireland, T.R.; Long, T.; Rienitz, O.; Pramann, A.; Wang, S.; Song, P.-S.; Wang, J. Molar mass measurement of a ²⁸Si-enriched silicon crystal with high precision secondary ion mass spectrometry (SIMS). *J. Anal. At. Spectrom.* **2022**, *37*, 2546–2555. [CrossRef]
59. Munteshari, O.; Zhou, Y.; Mei, B.-A.; Pilon, L. Theoretical validation of the step potential electrochemical spectroscopy (SPECS) and multiple potential step chronoamperometry (MUSCA) methods for pseudocapacitive electrodes. *Electrochim. Acta* **2019**, *321*, 134648. [CrossRef]
60. Palagonia, M.S.; Erinmwingbovo, C.; Brogioli, D.; La Mantia, F. Comparison between cyclic voltammetry and differential charge plots from galvanostatic cycling. *J. Electroanal. Chem.* **2019**, *847*, 113170. [CrossRef]
61. Nara, H.; Yokoshima, T.; Osaka, T. Technology of electrochemical impedance spectroscopy for an energy-sustainable society. *Curr. Opin. Electrochem.* **2020**, *20*, 66–77. [CrossRef]
62. Matsubara, Y. A Small yet Complete Framework for a Potentiostat, Galvanostat, and Electrochemical Impedance Spectrometer. *J. Chem. Educ.* **2021**, *98*, 3362–3370. [CrossRef]
63. Iwamoto, R.T.; Adams, R.N.; Lott, H. Drop-scale chronopotentiometry. *Anal. Chim. Acta* **1959**, *20*, 84–88. [CrossRef]
64. Lin, Y.; Lian, C.; Berrueta, M.U.; Liu, H.; van Roij, R. Microscopic Model for Cyclic Voltammetry of Porous Electrodes. *Phys. Rev. Lett.* **2022**, *128*, 206001. [CrossRef] [PubMed]
65. Lazanas, A.C.; Prodromidis, M.I. Electrochemical Impedance Spectroscopy—A Tutorial. *ACS Meas. Sci. Au* **2023**, *3*, 162–193. [CrossRef]
66. Moradighadi, N.; Nesic, S.; Tribollet, B. Identifying the dominant electrochemical reaction in electrochemical impedance spectroscopy. *Electrochim. Acta* **2021**, *400*, 139460. [CrossRef]
67. Cruz-Manzo, S.; Greenwood, P.; Chen, R. An Impedance Model for EIS Analysis of Nickel Metal Hydride Batteries. *J. Electrochem. Soc.* **2017**, *164*, A1446. [CrossRef]
68. Lindberg, A.; Eriksson, B.; Börjesson Axén, J.; Sandra, A.P.; Lindbergh, G. Gas phase composition of a NiMH battery during a work cycle. *RSC Adv.* **2024**, *14*, 19996–20003. [CrossRef]
69. Lota, K.; Swoboda, P.; Acznik, I.; Sierczyńska, A.; Mańczak, R.; Kolanowski, Ł.; Lota, G. Electrochemical properties of modified negative electrode for Ni-MH cell. *Curr. Appl. Phys.* **2020**, *20*, 106–113. [CrossRef]
70. Yang, C.C.; Wang, C.C.; Li, M.M.; Jiang, Q. A start of the renaissance for nickel metal hydride batteries: A hydrogen storage alloy series with an ultra-long cycle life. *J. Mater. Chem. A* **2017**, *5*, 1145–1152. [CrossRef]
71. Edalati, P.; Mohammadi, A.; Li, Y.; Li, H.-W.; Floriano, R.; Fuji, M.; Edalati, K. High-entropy alloys as anode materials of nickel-metal hydride batteries. *Scr. Mater.* **2022**, *209*, 114387. [CrossRef]
72. Wu, J.; Liu, Z.; Zhang, H.; Zou, Y.; Li, B.; Xiang, C.; Sun, L.; Xu, F.; Yu, T. Hydrogen storage performance of MgH₂ under catalysis by highly dispersed nickel-nanoparticle-doped hollow spherical vanadium nitride. *J. Magnes. Alloys* **2024**, *in press*. [CrossRef]
73. Rej, S.; Mascaretti, L.; Santiago, E.Y.; Tomanec, O.; Kment, Š.; Wang, Z.; Zbořil, R.; Fornasiero, P.; Govorov, A.O.; Naldoni, A. Determining Plasmonic Hot Electrons and Photothermal Effects during H₂ Evolution with TiN–Pt Nanohybrids. *ACS Catal.* **2020**, *10*, 5261–5271. [CrossRef]
74. Ross, D.J.; Halls, M.D.; Nazri, A.G.; Aroca, R.F. Raman scattering of complex sodium aluminum hydride for hydrogen storage. *Chem. Phys. Lett.* **2004**, *388*, 430–435. [CrossRef]
75. Alessandri, I.; Lombardi, J.R. Enhanced Raman Scattering with Dielectrics. *Chem. Rev.* **2016**, *116*, 14921–14981. [CrossRef]

76. Eslami, S.; Palomba, S. Integrated enhanced Raman scattering: A review. *Nano Conver.* **2021**, *8*, 41. [\[CrossRef\]](#)
77. Min, W.; Gao, X. The Duality of Raman Scattering. *Acc. Chem. Res.* **2024**, *57*, 1869–1905. [\[CrossRef\]](#)
78. Liebel, M.; Pazos-Perez, N.; van Hulst, N.F.; Alvarez-Puebla, R.A. Surface-enhanced Raman scattering holography. *Nat. Nanotechnol.* **2020**, *15*, 1005–1011. [\[CrossRef\]](#)
79. Balcerzak, M.; Runka, T.; Sniadecki, Z. Influence of carbon catalysts on the improvement of hydrogen storage properties in a body-centered cubic solid solution alloy. *Carbon* **2021**, *182*, 422–434. [\[CrossRef\]](#)
80. Vellingiri, L.; Annamalai, K.; Kandasamy, R.; Kombiah, I. Characterization and hydrogen storage properties of SnO₂ functionalized MWCNT nanocomposites. *Int. J. Hydrog. Energy* **2018**, *43*, 10396–10409. [\[CrossRef\]](#)
81. Reed, D.; Book, D. Recent applications of Raman spectroscopy to the study of complex hydrides for hydrogen storage. *Curr. Opin. Solid State Mater. Sci.* **2011**, *15*, 62–72. [\[CrossRef\]](#)
82. Valero-Pedraza, M.J.; Gascón, V.; Carreón, M.A.; Leardini, F.; Ares, J.R.; Martín, Á.; Sánchez-Sánchez, M.; Bañares, M.A. Operando Raman-mass spectrometry investigation of hydrogen release by thermolysis of ammonia borane confined in mesoporous materials. *Microporous Mesoporous Mater.* **2016**, *226*, 454–465. [\[CrossRef\]](#)
83. Lipinski, G.; Jeong, K.; Moritz, K.; Petermann, M.; May, E.F.; Stanwix, P.L.; Richter, M. Application of Raman Spectroscopy for Sorption Analysis of Functionalized Porous Materials. *Adv. Sci.* **2022**, *9*, 2105477. [\[CrossRef\]](#) [\[PubMed\]](#)
84. Liu, A.; Song, Y. In Situ High-Pressure and Low-Temperature Study of Ammonia Borane by Raman Spectroscopy. *J. Phys. Chem. C* **2012**, *116*, 2123–2131. [\[CrossRef\]](#)
85. Bleda-Martínez, M.J.; Pérez, J.M.; Linares-Solano, A.; Morallón, E.; Cazorla-Amorós, D. Effect of surface chemistry on electrochemical storage of hydrogen in porous carbon materials. *Carbon* **2008**, *46*, 1053–1059. [\[CrossRef\]](#)
86. Kalashnikov, D.A.; Paterova, A.V.; Kulik, S.P.; Krivitsky, L.A. Infrared spectroscopy with visible light. *Nat. Photonics* **2016**, *10*, 98–101. [\[CrossRef\]](#)
87. Lim, Y.; Hong, S.J.; Cho, Y.; Bang, J.; Lee, S. Fourier Surfaces Reaching Full-Color Diffraction Limits. *Adv. Mater.* **2024**, *36*, e2404540. [\[CrossRef\]](#)
88. Hashimoto, K.; Nakamura, T.; Kageyama, T.; Badarla, V.R.; Shimada, H.; Horisaki, R.; Ideguchi, T. Upconversion time-stretch infrared spectroscopy. *Light Sci. Appl.* **2023**, *12*, 48. [\[CrossRef\]](#)
89. Lassaline, N.; Brechbühler, R.; Vonk, S.J.W.; Ridderbeek, K.; Spieser, M.; Bisig, S.; le Feber, B.; Rabouw, F.T.; Norris, D.J. Optical Fourier surfaces. *Nature* **2020**, *582*, 506–510. [\[CrossRef\]](#)
90. Muthu, R.N.; Rajashabala, S.; Kannan, R. Hydrogen storage performance of lithium borohydride decorated activated hexagonal boron nitride nanocomposite for fuel cell applications. *Int. J. Hydrog. Energy* **2017**, *42*, 15586–15596. [\[CrossRef\]](#)
91. Pei, Z.; Bai, Y.; Wang, Y.; Wu, F.; Wu, C. Insight to the Thermal Decomposition and Hydrogen Desorption Behaviors of NaNH₂–NaBH₄ Hydrogen Storage Composite. *ACS Appl. Mater. Interfaces* **2017**, *9*, 31977–31984. [\[CrossRef\]](#)
92. Kern, J.; Alonso-Mori, R.; Tran, R.; Hattne, J.; Gildea, R.J.; Echols, N.; Glöckner, C.; Hellmich, J.; Laksmono, H.; Sierra, R.G.; et al. Simultaneous Femtosecond X-ray Spectroscopy and Diffraction of Photosystem II at Room Temperature. *Science* **2013**, *340*, 491–495. [\[CrossRef\]](#) [\[PubMed\]](#)
93. McCusker, L.B. Electron diffraction and the hydrogen atom. *Science* **2017**, *355*, 136. [\[CrossRef\]](#) [\[PubMed\]](#)
94. Wang, Y.; Lan, Z.; Huang, X.; Liu, H.; Guo, J. Study on catalytic effect and mechanism of MOF (MOF = ZIF-8, ZIF-67, MOF-74) on hydrogen storage properties of magnesium. *Int. J. Hydrog. Energy* **2019**, *44*, 28863–28873. [\[CrossRef\]](#)
95. Ma, Z.; Zhang, Q.; Panda, S.; Zhu, W.; Sun, F.; Khan, D.; Dong, J.; Ding, W.; Zou, J. In situ catalyzed and nanoconfined magnesium hydride nanocrystals in a Ni-MOF scaffold for hydrogen storage. *Sustain. Energy Fuels* **2020**, *4*, 4694–4703. [\[CrossRef\]](#)
96. Zhang, L.; Nyahuma, F.M.; Zhang, H.; Cheng, C.; Zheng, J.; Wu, F.; Chen, L. Metal organic framework supported niobium pentoxide nanoparticles with exceptional catalytic effect on hydrogen storage behavior of MgH₂. *Green Energy Environ.* **2023**, *8*, 589–600. [\[CrossRef\]](#)
97. Chen, L.; Wang, B.; Zhang, W.; Zheng, S.; Chen, Z.; Zhang, M.; Dong, C.; Pan, F.; Li, S. Crystal Structure Assignment for Unknown Compounds from X-ray Diffraction Patterns with Deep Learning. *J. Am. Chem. Soc.* **2024**, *146*, 8098–8109. [\[CrossRef\]](#)
98. Zlotea, C.; Sow, M.A.; Ek, G.; Couzinié, J.P.; Perrière, L.; Guillot, I.; Bourgon, J.; Møller, K.T.; Jensen, T.R.; Akiba, E.; et al. Hydrogen sorption in TiZrNbHfTa high entropy alloy. *J. Alloys Compd.* **2019**, *775*, 667–674. [\[CrossRef\]](#)
99. Jensen, T.R.; Andreasen, A.; Vegge, T.; Andreasen, J.W.; Ståhl, K.; Pedersen, A.S.; Nielsen, M.M.; Molenbroek, A.M.; Besenbacher, F. Dehydrogenation kinetics of pure and nickel-doped magnesium hydride investigated by in situ time-resolved powder X-ray diffraction. *Int. J. Hydrog. Energy* **2006**, *31*, 2052–2062. [\[CrossRef\]](#)
100. Dewhurst, C.D.; Grillo, I. Neutron imaging using a conventional small-angle neutron scattering instrument. *J. Appl. Crystallogr.* **2016**, *49*, 736–742. [\[CrossRef\]](#)
101. Zu, T.; Tang, Y.; Huang, Z.; Qin, S.; Li, J.; He, Q.; Cao, L.; Wu, H. Treatments of Thermal Neutron Scattering Data and Their Effect on Neutronics Calculations. *Front. Energy Res.* **2021**, *9*, 779261. [\[CrossRef\]](#)
102. Mühlbauer, S.; Honecker, D.; Périgo, E.A.; Bergner, F.; Disch, S.; Heinemann, A.; Erokhin, S.; Berkov, D.; Leighton, C.; Eskildsen, M.R.; et al. Magnetic small-angle neutron scattering. *Rev. Mod. Phys.* **2019**, *91*, 015004. [\[CrossRef\]](#)
103. Nazirkar, N.P.; Shi, X.; Shi, J.; N’Gom, M.; Fohtung, E. Coherent diffractive imaging with twisted X-rays: Principles, applications, and outlook. *Appl. Phys. Rev.* **2024**, *11*, 021302. [\[CrossRef\]](#)
104. Cao, C.; Toney, M.F.; Sham, T.-K.; Harder, R.; Shearing, P.R.; Xiao, X.; Wang, J. Emerging X-ray imaging technologies for energy materials. *Mater. Today* **2020**, *34*, 132–147. [\[CrossRef\]](#)

105. Schriber, E.A.; Paley, D.W.; Bolotovskiy, R.; Rosenberg, D.J.; Sierra, R.G.; Aquila, A.; Mendez, D.; Poitevin, F.; Blaschke, J.P.; Bhowmick, A.; et al. Chemical crystallography by serial femtosecond X-ray diffraction. *Nature* **2022**, *601*, 360–365. [\[CrossRef\]](#)
106. Yu, X.; Cheng, Y.; Li, Y.; Polo-Garzon, F.; Liu, J.; Mamontov, E.; Li, M.; Lennon, D.; Parker, S.F.; Ramirez-Cuesta, A.J.; et al. Neutron Scattering Studies of Heterogeneous Catalysis. *Chem. Rev.* **2023**, *123*, 8638–8700. [\[CrossRef\]](#)
107. Ponthieu, M.; Cuevas, F.; Fernández, J.F.; Laversenne, L.; Porcher, F.; Latroche, M. Structural Properties and Reversible Deuterium Loading of MgD₂–TiD₂ Nanocomposites. *J. Phys. Chem. C* **2013**, *117*, 18851–18862. [\[CrossRef\]](#)
108. Ramirez-Cuesta, A.J.; Jones, M.O.; David, W.I.F. Neutron scattering and hydrogen storage. *Mater. Today* **2009**, *12*, 54–61. [\[CrossRef\]](#)
109. Sato, T.; Orimo, S.-I. Hydrogen Vibration in Hydrogen Storage Materials Investigated by Inelastic Neutron Scattering. *Top. Catal.* **2021**, *64*, 614–621. [\[CrossRef\]](#)
110. Zhang, X.; Sun, Y.; Xia, G.; Yu, X. Light-weight solid-state hydrogen storage materials characterized by neutron scattering. *J. Alloys Compd.* **2022**, *899*, 163254. [\[CrossRef\]](#)
111. Jeffries, C.M.; Ilavsky, J.; Martel, A.; Hinrichs, S.; Meyer, A.; Pedersen, J.S.; Sokolova, A.V.; Svergun, D.I. Small-angle X-ray and neutron scattering. *Nat. Rev. Methods Primers* **2021**, *1*, 70. [\[CrossRef\]](#)
112. Yusuf, S.M.; Kumar, A. Neutron scattering of advanced magnetic materials. *Appl. Phys. Rev.* **2017**, *4*, 031303. [\[CrossRef\]](#)
113. Korin, E.; Froumin, N.; Cohen, S. Surface Analysis of Nanocomplexes by X-ray Photoelectron Spectroscopy (XPS). *ACS Biomater. Sci. Eng.* **2017**, *3*, 882–889. [\[CrossRef\]](#) [\[PubMed\]](#)
114. Greczynski, G.; Hultman, L. X-ray photoelectron spectroscopy: Towards reliable binding energy referencing. *Prog. Mater. Sci.* **2020**, *107*, 100591. [\[CrossRef\]](#)
115. Das, T.K.; Banerjee, S.; Sharma, P.; Sudarsan, V.; Sastry, P.U. Nitrogen doped porous carbon derived from EDTA: Effect of pores on hydrogen storage properties. *Int. J. Hydrog. Energy* **2018**, *43*, 8385–8394. [\[CrossRef\]](#)
116. Pei, P.; Whitwick, M.B.; Kureshi, S.; Cannon, M.; Quan, G.; Kjeang, E. Hydrogen storage mechanism in transition metal decorated graphene oxide: The symbiotic effect of oxygen groups and high layer spacing. *Int. J. Hydrog. Energy* **2020**, *45*, 6713–6726. [\[CrossRef\]](#)
117. Zhao, Y.; Liu, F.; Tan, J.; Li, P.; Wang, Z.; Zhu, K.; Mai, X.; Liu, H.; Wang, X.; Ma, Y.; et al. Preparation and hydrogen storage of Pd/MIL-101 nanocomposites. *J. Alloys Compd.* **2019**, *772*, 186–192. [\[CrossRef\]](#)
118. Smardz, L.; Nowak, M.; Jurczyk, M. XPS valence band studies of hydrogen storage nanocomposites. *Int. J. Hydrog. Energy* **2012**, *37*, 3659–3664. [\[CrossRef\]](#)
119. Kumar, S.; Kojima, Y.; Kain, V. XPS study on the vanadocene-magnesium system to understand the hydrogen sorption reaction mechanism under room temperature. *Int. J. Hydrog. Energy* **2019**, *44*, 2981–2987. [\[CrossRef\]](#)
120. Selvam, P.; Viswanathan, B.; Srinivasan, V. XPS and XAES studies on hydrogen storage magnesium-based alloys. *Int. J. Hydrog. Energy* **1989**, *14*, 899–902. [\[CrossRef\]](#)
121. Xing, X.; Liu, Y.; Zhang, Z.; Liu, T. Hierarchical Structure Carbon-Coated CoNi Nanocatalysts Derived from Flower-Like Bimetal MOFs: Enhancing the Hydrogen Storage Performance of MgH₂ under Mild Conditions. *ACS Sustain. Chem. Eng.* **2023**, *11*, 4825–4837. [\[CrossRef\]](#)
122. Xie, X.; Zhang, B.; Kimura, H.; Ni, C.; Yu, R.; Du, W. Morphology evolution of bimetallic Ni/Zn-MOFs and derived Ni₃ZnCo_{0.7}/Ni/ZnO used to destabilize MgH₂. *Chem. Eng. J.* **2023**, *464*, 142630. [\[CrossRef\]](#)
123. Zhang, J.; Wang, W.; Chen, X.; Jin, J.; Yan, X.; Huang, J. Single-Atom Ni Supported on TiO₂ for Catalyzing Hydrogen Storage in MgH₂. *J. Am. Chem. Soc.* **2024**, *146*, 10432–10442. [\[CrossRef\]](#) [\[PubMed\]](#)
124. Silva, B.H.; Almeida, J.M.; Hernandez, A.C.; Goncalves, R.V.; Zepon, G. Pulsed laser activation method for hydrogen storage alloys. *Int. J. Hydrog. Energy* **2024**, *53*, 885–890. [\[CrossRef\]](#)
125. Barroo, C.; Wang, Z.-J.; Schlögl, R.; Willinger, M.-G. Imaging the dynamics of catalysed surface reactions by in situ scanning electron microscopy. *Nat. Catal.* **2019**, *3*, 30–39. [\[CrossRef\]](#)
126. Bianco, E.; Kourkoutis, L.F. Atomic-Resolution Cryogenic Scanning Transmission Electron Microscopy for Quantum Materials. *Acc. Chem. Res.* **2021**, *54*, 3277–3287. [\[CrossRef\]](#)
127. Kim, P.Y.; Ribbe, A.E.; Russell, T.P.; Hoagland, D.A. Visualizing the Dynamics of Nanoparticles in Liquids by Scanning Electron Microscopy. *ACS Nano* **2016**, *10*, 6257–6264. [\[CrossRef\]](#)
128. Donald, A.M. The use of environmental scanning electron microscopy for imaging wet and insulating materials. *Nat. Mater.* **2003**, *2*, 511–516. [\[CrossRef\]](#)
129. McKernan, S. Environmental Scanning Electron Microscopy:—Advantages and Disadvantages. *Microsc. Microanal.* **1997**, *3*, 381–382. [\[CrossRef\]](#)
130. Niania, M.; Podor, R.; Britton, T.B.; Li, C.; Cooper, S.J.; Svetkov, N.; Skinner, S.; Kilner, J. Correction: In situ study of strontium segregation in La_{0.6}Sr_{0.4}Co_{0.2}Fe_{0.8}O_{3–δ} in ambient atmospheres using high-temperature environmental scanning electron microscopy. *J. Mater. Chem. A* **2018**, *6*, 14464. [\[CrossRef\]](#)
131. Zhang, L.; Zhu, J.; Wilke, K.L.; Xu, Z.; Zhao, L.; Lu, Z.; Goddard, L.L.; Wang, E.N. Enhanced Environmental Scanning Electron Microscopy Using Phase Reconstruction and Its Application in Condensation. *ACS Nano* **2019**, *13*, 1953–1960. [\[CrossRef\]](#)
132. Zhu, J.; Zhang, L.; Li, X.; Wilke, K.L.; Wang, E.N.; Goddard, L.L. Quasi-Newtonian Environmental Scanning Electron Microscopy (QN-ESEM) for Monitoring Material Dynamics in High-Pressure Gaseous Environments. *Adv. Sci.* **2020**, *7*, 2001268. [\[CrossRef\]](#) [\[PubMed\]](#)

133. Ren, L.; Zhu, W.; Zhang, Q.; Lu, C.; Sun, F.; Lin, X.; Zou, J. MgH₂ confinement in MOF-derived N-doped porous carbon nanofibers for enhanced hydrogen storage. *Chem. Eng. J.* **2022**, *434*, 134701. [\[CrossRef\]](#)
134. Schulz, F.; Ritala, J.; Krejci, O.; Seitsonen, A.P.; Foster, A.S.; Liljeroth, P. Elemental Identification by Combining Atomic Force Microscopy and Kelvin Probe Force Microscopy. *ACS Nano* **2018**, *12*, 5274–5283. [\[CrossRef\]](#) [\[PubMed\]](#)
135. Collins, L.; Liu, Y.; Ovchinnikova, O.S.; Proksch, R. Quantitative Electromechanical Atomic Force Microscopy. *ACS Nano* **2019**, *13*, 8055–8066. [\[CrossRef\]](#)
136. Oinonen, N.; Xu, C.; Alldritt, B.; Canova, F.F.; Urtev, F.; Cai, S.; Krejci, O.; Kannala, J.; Liljeroth, P.; Foster, A.S. Electrostatic Discovery Atomic Force Microscopy. *ACS Nano* **2022**, *16*, 89–97. [\[CrossRef\]](#)
137. Singh, A. Towards resolving proteomes in single cells. *Nat. Methods* **2021**, *18*, 856. [\[CrossRef\]](#)
138. Songen, H.; Bechstein, R.; Kuhnle, A. Quantitative atomic force microscopy. *J. Phys. Condens. Matter* **2017**, *29*, 274001. [\[CrossRef\]](#)
139. Kalisvaart, W.P.; Lubber, E.J.; Poirier, E.; Harrower, C.T.; Teichert, A.; Wallacher, D.; Grimm, N.; Steitz, R.; Fritzsche, H.; Mitlin, D. Probing the Room Temperature Deuterium Absorption Kinetics in Nanoscale Magnesium Based Hydrogen Storage Multilayers Using Neutron Reflectometry, X-ray Diffraction, and Atomic Force Microscopy. *J. Phys. Chem. C* **2012**, *116*, 5868–5880. [\[CrossRef\]](#)
140. Ke, X.; Zhang, M.; Zhao, K.; Su, D. Moire Fringe Method via Scanning Transmission Electron Microscopy. *Small Methods* **2022**, *6*, e2101040. [\[CrossRef\]](#)
141. Kuei, B.; Aplan, M.P.; Litofsky, J.H.; Gomez, E.D. New opportunities in transmission electron microscopy of polymers. *Mater. Sci. Eng. R Rep.* **2020**, *139*, 100516. [\[CrossRef\]](#)
142. Lei, X.; Zhao, J.; Wang, J.; Su, D. Tracking lithiation with transmission electron microscopy. *Sci. China Chem.* **2023**, *67*, 291–311. [\[CrossRef\]](#)
143. Schwartz, O.; Axelrod, J.J.; Campbell, S.L.; Turnbaugh, C.; Glaeser, R.M.; Muller, H. Laser phase plate for transmission electron microscopy. *Nat Methods* **2019**, *16*, 1016–1020. [\[CrossRef\]](#) [\[PubMed\]](#)
144. Dick, K.A. Gas-phase materials synthesis in environmental transmission electron microscopy. *MRS Bull.* **2023**, *48*, 833–841. [\[CrossRef\]](#)
145. Han, Z.; Yang, F.; Li, Y. Dynamics of metal-support interface revealed by environmental transmission electron microscopy. *Matter* **2022**, *5*, 2531–2533. [\[CrossRef\]](#)
146. Parent, L.R.; Pham, C.H.; Patterson, J.P.; Denny, M.S.; Cohen, S.M.; Gianneschi, N.C.; Paesani, F. Pore Breathing of Metal-Organic Frameworks by Environmental Transmission Electron Microscopy. *J. Am. Chem. Soc.* **2017**, *139*, 13973–13976. [\[CrossRef\]](#)
147. Stach, E.A.; Zakharov, D.; Akatay, M.C.; Baumann, P.; Ribeiro, F.; Zvienevich, Y.; Li, Y.; Frenkel, A. Developments in environmental transmission electron microscopy for catalysis research. *Microsc. Microanal.* **2013**, *19*, 1174–1175. [\[CrossRef\]](#)
148. Tanaka, N.; Fujita, T.; Takahashi, Y.; Yamasaki, J.; Murata, K.; Arai, S. Progress in environmental high-voltage transmission electron microscopy for nanomaterials. *Philos. Trans. R. Soc. A Math. Phys. Eng. Sci.* **2020**, *378*, 20190602. [\[CrossRef\]](#)
149. Nakamura, E.; Sommerdijk, N.; Zheng, H. Transmission Electron Microscopy for Chemists. *Acc. Chem. Res.* **2017**, *50*, 1795–1796. [\[CrossRef\]](#)
150. Wu, R.; Zhang, X.; Liu, Y.; Zhang, L.; Hu, J.; Gao, M.; Pan, H. A Unique Double-Layered Carbon Nanobowl-Confined Lithium Borohydride for Highly Reversible Hydrogen Storage. *Small* **2020**, *16*, 2001963. [\[CrossRef\]](#)
151. Liu, X.; Zhang, C.; Li, Y.; Niemantsverdriet, J.W.; Wagner, J.B.; Hansen, T.W. Environmental Transmission Electron Microscopy (ETEM) Studies of Single Iron Nanoparticle Carburization in Synthesis Gas. *ACS Catal.* **2017**, *7*, 4867–4875. [\[CrossRef\]](#)
152. Zhang, D.; Jin, C.; Li, Z.Y.; Zhang, Z.; Li, J. Oxidation behavior of cobalt nanoparticles studied by in situ environmental transmission electron microscopy. *Sci. Bull.* **2017**, *62*, 775–778. [\[CrossRef\]](#) [\[PubMed\]](#)
153. Adams, J.D.; Erickson, B.W.; Grossenbacher, J.; Brugger, J.; Nievergelt, A.; Fantner, G.E. Harnessing the damping properties of materials for high-speed atomic force microscopy. *Nat. Nanotechnol.* **2016**, *11*, 147–151. [\[CrossRef\]](#) [\[PubMed\]](#)
154. Ando, T. High-speed atomic force microscopy. *Curr. Opin. Chem. Biol.* **2019**, *51*, 105–112. [\[CrossRef\]](#) [\[PubMed\]](#)
155. Brown, B.P.; Picco, L.; Miles, M.J.; Faul, C.F.J. Opportunities in High-Speed Atomic Force Microscopy. *Small* **2013**, *9*, 3201–3211. [\[CrossRef\]](#)
156. Fukui, T.; Uchihashi, T.; Sasaki, N.; Watanabe, H.; Takeuchi, M.; Sugiyasu, K. Direct Observation and Manipulation of Supramolecular Polymerization by High-Speed Atomic Force Microscopy. *Angew. Chem. Int. Ed.* **2018**, *57*, 15465–15470. [\[CrossRef\]](#)
157. Das, S.K.; Badal, F.R.; Rahman, M.A.; Islam, M.A.; Sarker, S.K.; Paul, N. Improvement of Alternative Non-Raster Scanning Methods for High Speed Atomic Force Microscopy: A Review. *IEEE Access* **2019**, *7*, 115603–115624. [\[CrossRef\]](#)
158. Verma, A.; Wilson, N.; Joshi, K. Solid state hydrogen storage: Decoding the path through machine learning. *Int. J. Hydrog. Energy* **2024**, *50*, 1518–1528. [\[CrossRef\]](#)

Disclaimer/Publisher's Note: The statements, opinions and data contained in all publications are solely those of the individual author(s) and contributor(s) and not of MDPI and/or the editor(s). MDPI and/or the editor(s) disclaim responsibility for any injury to people or property resulting from any ideas, methods, instructions or products referred to in the content.